IVYSPRING INTERNATIONAL PUBLISHER

Theranostics

2024; 14(7): 2881-2896. doi: 10.7150/thno.95383

Research Paper

Distinct eLPB^{ChAT} projections for methamphetamine withdrawal anxiety and primed reinstatement of conditioned place preference

Wenwen Chen[1,*], Hao Guo[1,*], Ning Zhou[1,*], Yuning Mai[1], Tao Hu[1], Xing Xu[1], Teng He[1], Jun Wen[1], Shan Qin[2], Chengyong Liu[2], Wenzhong Wu[2], Hee Young Kim[3], Yu Fan[1,✉], Feifei Ge[1,✉], Xiaowei Guan[1,✉]

1. Department of Human Anatomy and Histoembryology, Nanjing University of Chinese Medicine, Nanjing, China.
2. Department of Acupuncture-Moxibustion and Rehabilitation, Jiangsu Province Hospital of Chinese Medicine, Affiliated Hospital of Nanjing University of Chinese Medicine, Nanjing, China.
3. Department of Physiology, Yonsei University College of Medicine, Seoul, South Korea.

* These authors equally contributed to this work.

✉ Corresponding authors: guanxw918@njucm.edu.cn (XG), yfan@njucm.edu.cn (YF), ffge@njucm.edu.cn (FG).

Received: 2024.02.16; Accepted: 2024.04.24; Published: 2024.04.29

Abstract

Methamphetamine (METH) withdrawal anxiety symptom and relapse have been significant challenges for clinical practice, however, the underlying neuronal basis remains unclear. Our recent research has identified a specific subpopulation of choline acetyltransferase (ChAT$^+$) neurons localized in the external lateral portion of parabrachial nucleus (eLPB^{ChAT}), which modulates METH primed-reinstatement of conditioned place preference (CPP). Here, the anatomical structures and functional roles of eLPB^{ChAT} projections in METH withdrawal anxiety and primed reinstatement were further explored.

Methods: In the present study, a multifaceted approach was employed to dissect the LPB^{ChAT+} projections in male mice, including anterograde and retrograde tracing, acetylcholine (Ach) indicator combined with fiber photometry recording, photogenetic and chemogenetic regulation, as well as electrophysiological recording. METH withdrawal anxiety-like behaviors and METH-primed reinstatement of conditioned place preference (CPP) were assessed in male mice.

Results: We identified that eLPB^{ChAT} send projections to PKCδ-positive (PKCδ$^+$) neurons in lateral portion of central nucleus of amygdala (lCeA^{PKCδ}) and oval portion of bed nucleus of the stria terminalis (ovBNST^{PKCδ}), forming eLPB^{ChAT}–lCeA^{PKCδ} and eLPB^{ChAT}–ovBNST^{PKCδ} pathways. At least in part, the eLPB^{ChAT} neurons positively innervate lCeA^{PKCδ} neurons and ovBNST^{PKCδ} neurons through regulating synaptic elements of presynaptic Ach release and postsynaptic nicotinic acetylcholine receptors (nAChRs). METH withdrawal anxiety and METH-primed reinstatement of CPP respectively recruit eLPB^{ChAT}–lCeA^{PKCδ} pathway and eLPB^{ChAT}–ovBNST^{PKCδ} pathway in male mice.

Conclusion: Our findings put new insights into the complex neural networks, especially focusing on the eLPB^{ChAT} projections. The eLPB^{ChAT} is a critical node in the neural networks governing METH withdrawal anxiety and primed-reinstatement of CPP through its projections to the lCeA^{PKCδ} and ovBNST^{PKCδ}, respectively.

Keywords: eLPB^{ChAT}–lCeA^{PKCδ}; eLPB^{ChAT}–ovBNST^{PKCδ}; methamphetamine; anxiety; conditioned place preference

Introduction

Methamphetamine (METH) is a highly addictive and widely abused psychostimulant drug. Among individuals with METH use disorders (MUD), it has been observed that 34.3% develop withdrawal anxiety symptoms [1, 2], and up to 90% are estimated to relapse [3], posing a significant challenge for clinical practice.

The parabrachial nucleus (PBN), being located within the pons, functions as an integrator of sensory input from the surrounding environment and subsequently relays this information to forebrain structures. The majority of PBN neurons are

excitatory features [4, 5], being positively correlated with behaviors indicative of pain [6-8], itch [9, 10], fear [11], aversive [12], and emotion [10, 13]. Our recent research has identified a specific subpopulation of choline acetyltransferase ($ChAT^+$) neurons located in the PBN, specifically within the external lateral portion of PBN ($eLPB^{ChAT}$) [14]. These neurons play a crucial role in modulating METH-primed reinstatement of METH conditioned place preference (CPP) in male mice. However, the precise structures and functions of $eLPB^{ChAT}$ projections have not yet to be explored.

The LPB predominately send projections to the thalamus and limbic nuclei, such as the central nucleus of the amygdala (CeA) [6, 8, 13] and the bed nucleus of the stria terminalis (BNST) [6, 15, 16], both of which are pivotal in anxiety [13, 17] and addiction [18-20]. The activation of projections from the LPB to the CeA or BNST elicits aversive responses [6]. Given its potential as a target for anxiolytic agents, the CeA is implicated in the emotional component of the behavioral reaction to alcohol, particularly anxiety [21, 22]. Activation of LPB–CeA pathway alone was sufficient to induced anxiety-like behavior in mice [13]. It is noteworthy that social choice-induced abstinence has been found to prevent the incubation of METH craving, which was associated with the activation of protein kinase C delta-positive neurons in the CeA ($CeA^{PKC\delta}$) [19]. Furthermore, withdrawal from METH has been shown to increase the activity of BNST neurons [23], and $BNST^{PKC\delta}$ neurons are also activated by aversive conditions to promote anxiety-like behavior [17]. Based on the mapping results obtained from fMOST [14], our previous findings have identified two distinct groups of $eLPB^{ChAT}$ efferent neurons projecting to the CeA and BNST. Taken together, we aimed to gain a more comprehensive understanding of LPB^{ChAT+} projections and their potential contribution to METH-related behaviors.

In the present study, a multifaceted approach was employed to dissect the LPB^{ChAT+} projections in mice, including anterograde and retrograde tracing, acetylcholine (Ach) indicator combined with fiber photometry recording, as well as electrophysiological recording. We first identified the structural connectivity and physiological innervation of $eLPB^{ChAT}$–CeA pathway and $eLPB^{ChAT}$–BNST pathway in naïve male mice. Then, we explored the role of $eLPB^{ChAT}$–CeA pathway and $eLPB^{ChAT}$–BNST pathway in the anxiety-like behaviors during METH withdrawal period and METH-primed reinstatement of CPP in male mice. Our findings put new insights into the complex neural networks, especially focusing on the $eLPB^{ChAT}$ projections, that contribute to the METH withdrawal anxiety and primed reinstatement of CPP.

Materials and methods

Animals

Male C57BL/6 wild type (WT) and *ChAT-Cre* male mice weighing 22-25 g (9 weeks old) were used. All animals were housed at constant humidity (40~60%) and temperature (24 ± 2ºC) with a 12-hour light/dark cycle (lights on at 8 a.m.) and allowed free access to food and water. All male mice were handled for three days before onset of experiments. The naive male mice utilized in this experiment were not subjected to any drug treatment or behavioral training, and had an initial weight range of 22-25g (9 weeks old). All procedures were carried out in accordance with the National Institutes of Health Guide for the Care and Use of Laboratory Animals and approved by the Institutional Animal Care and Use Committee (IACUC) at Nanjing University of Chinese Medicine, China.

Immunofluorescence

The male mice were deeply anesthetized with 10% chloral hydrate (0.2 ml, i.p.) and sequentially perfused with 0.9% saline and 4% paraformaldehyde (PFA). The brains were removed and post-fixed in 4% PFA at 4 °C overnight. After dehydration of the brains with 30% (w/v) sucrose, coronal brain sections (30 μm) were cut on a cryostat (Leica, Germany) and used for immunofluorescence. The sections were incubated in 0.3% (v/v) Triton X-100 for 0.5 h, blocked with 5% donkey serum for 1.5 h at room temperature, and incubated overnight at 4°C with the following primary antibodies: goat anti-ChAT (1:200, RRID: AB_2079751, Millipore, USA), mouse anti-NeuN (1:800, RRID: AB_2298772, Millipore, USA), guinea pig anti-c-Fos (1:3000, RRID: AB_2905595, Synaptic System, USA), rabbit anti-c-Fos (1:2000, RRID: AB_2247211, Cell Signaling Technology, USA), mouse anti-c-Fos (1:1500, RRID: AB_2747772, Abcam, USA) and rabbit anti-PKCδ (1:1000, RRID: None, HuaBio, China), followed by the corresponding fluorophore-conjugated secondary antibodies for 1.5 h at room temperature. The following secondary antibodies were used here: Alexa Fluor 488-labeled donkey anti-rabbit secondary antibody (1:500, RRID: AB_2762833, Invitrogen, USA), Alexa Fluor 488-labeled donkey anti-mouse secondary antibody (1:500, RRID: AB_141607, Invitrogen, USA), Alexa Fluor 555-labeled goat anti-guinea pig secondary antibody (1:500, RRID: None, Abcam, USA), Alexa Fluor 555-labeled donkey anti-rabbit secondary antibody (1:500, RRID: AB_2762834, Invitrogen, USA), Alexa Fluor 555-labeled donkey anti-mouse

secondary antibody (1:500, RRID: AB_2762848, Invitrogen, USA), Alexa Fluor 555-labeled donkey anti-goat secondary antibody (1:500, RRID: AB_2762839, Invitrogen, USA), DyLight™ 680-labeled goat anti-guinea pig secondary antibody (1:500, RRID: AB_2556678, Invitrogen, USA), Alexa Fluor 680-labeled donkey anti-rabbit secondary antibody (1:500, RRID: AB_2762836, Invitrogen, USA), Alexa Fluor 680-labeled donkey anti-mouse secondary antibody (1:500, RRID: AB_2762831, Invitrogen, USA), Alexa Fluor 680-labeled donkey anti-goat secondary antibody (1:500, RRID: AB_2762841, Invitrogen, USA). In detail of the staining for c-Fos and PKCδ in the lCeA or ovBNST, brain slices were attached to slides and placed in an oven at 60°C for 30 min, and then immersed in 4% PFA solution for 15 min in a refrigerator at 4°C for fixation. Then graded concentration alcohol dehydration (50%-70%-100%-100%) was performed sequentially for 5 min each time. Next, antigen repair was performed by immersing the slides with brain slices attached in 10 mM PH=6.0 trisodium citrate solution and heating in a water bath at 82°C for 30 min. Normal staining steps were then followed. Fluorescence signals were captured by TCS SP8 confocal microscope (Leica, Germany), and STELLARIS 8 DIVE confocal microscope (Leica, Germany).

Tracing virus injection

All viruses in the present study were packaged by BrainVTA (China). The male mice were fixed in a stereotactic frame (RWD, China) under 2% isoflurane anesthesia. A heating pad was used to maintain the body temperature of the mice at 37 °C. Unless otherwise noted, a volume of 100 nl virus was injected per side. The injections were given over 5 min at a rate of 20 nl/min by an infusion pump (Drummond, USA) and left in place for 10 min. The stereotaxic coordinates for the eLPB are used as following: AP, - 5.07/5.19/5.33 mm, ML, ± 1.45 mm and DV, - 3.30 mm. The stereotaxic coordinates of the lCeA are used as following: AP, - 1.31 mm; ML, ± 2.90 mm; DV, - 4.50 mm. The stereotaxic coordinates for the ovBNST are used as following: AP, + 0.13 mm, ML, ± 1.1mm, and DV, - 4.05 mm. For anterograde tracing, the *rAAV2/9-EF1a-DIO-EGFP* (PT-0795, 2.04E+12 vg/ml, BrainVTA, China) virus was injected into the unilateral eLPB of ChAT-Cre mice. For retrograde tracing, the CTB-555 (CTB-02, 1 μg/μl, BrainVTA, China) was injected into the unilateral lCeA and ovBNST of WT mice. After 1-week (retrograde tracing) and 3/4-week (anterograde tracing) transfection, male mice were perfused with 0.9% saline, followed by 4% PFA and then images of the CTB-555 or EGFP signals were visualized to assess the virus-injected positions. Animals with missed injections were excluded from the study.

Fiber photometry

On WT male mice, the *rAAV2/9-hSyn-Ach3.0* (PT-1335, 5.68E+12 vg/mL, BrainVTA, China) virus was unilaterally injected into the lCeA (AP, - 1.31 mm; ML, - 2.90 mm; DV, - 4.50 mm) or ovBNST (AP + 0.13 mm, ML - 1.1mm, DV - 4.05 mm), while the *rAAV2/9-ChAT-hM3D(Gq)-mCherry* (PT-2213, 5.54E+12 vg/ml, BrainVTA, China) or *rAAV2/9-ChAT-hM4D(Gi)-mCherry* (PT-3108, 6.28E+12 vg/ml, BrainVTA, China) virus was bilaterally injected into the eLPB (AP, - 5.19 mm, ML, ± 1.45 mm and DV, - 3.30 mm). An optical fiber (200 μm outer diameter, 0.37 numerical aperture, Thinkerbiotech, China) was placed 100 μm above the viral injection site. After 3 weeks, the calcium-dependent fluorescence signals of Ach 3.0 sensor in the lCeA or ovBNST were recorded at homecage. The signals were obtained by stimulating cells that transfected Ach3.0 sensor using a 470 nm LED (35-40 μW at fiber tip), while calcium-independent signals were obtained by stimulating these cells with a 405 nm LED (15-20 μW at fiber tip). The LED lights of 470 nm and 405 nm were alternated at 66 fps and light emission was recorded using sCMOS camera containing the entire fiber bundle (2 m in length, NA = 0.37, 200 μm core, Thinkerbiotech, China). The analog voltage signals fluorescent was filtered at 30 Hz and digitalized at 100 Hz. The Ach3.0 signals were recorded and analyzed by ThinkerTech TrippleColor MultiChannel fiber photometry Acquisition Software and ThinkerTech TrippleColor MultiChannel fiber photometry Analysis Package (Thinkerbiotech, China), respectively. The raw heatmap data were normalized by Z-Score normalization. The formula for Z-Score is $(D - \mu)/\sigma$, where D is the raw fiber photometry signal data, μ is the mean value of raw data and σ is the standard deviation of raw data. The baseline fluorescence signal which was recorded for 5 min with 1 min record and 4 min interval (1 session) prior to clozapine-N-oxide (CNO, Selleck, USA) treatment. The real-time fluorescence signal which was recorded for 60 min with a 1-min recording and 4-min interval (11 session). The raw heatmap data from one mouse was merged as a statistical point and normalized using area under the curve (AUC) normalization. The AUC represents the integral under the recording duration relative to the corresponding baseline at each trial. For the immunofluorescence experiment, another set of same mice models was utilized, the brain tissue was collected at 35 min after CNO injection.

Electrophysiology

The *rAAV2/9-ChAT-CRE-P2A-EGFP-WPRE-hGH* polyA (PT-0652, 5.30E+12 vg/mL, BrainVTA, China) and *rAAV2/9-Ef1a-DIO-hChR2-mCherry-WPRE-hGH pA* (PT-0002, 5.05E+12 vg/mL, BrainVTA, China) virus was bilaterally injected into the eLPB of WT mice. The mice (n = 6 mice) were deeply anesthetized with isoflurane (RWD, China) and perfused with ice-cold cutting solution. Slice preparation was performed as previously described [2]. Slices containing the lCeA or ovBNST were cut at a 200 μm thickness using a vibratome in 4°C cutting solution. The slices were transferred to 37°C cutting solution for 9 min, then transferred to a holding solution to allow for recovery at room temperature for 1 h before recordings. Throughout the electrophysiological recordings, the slices were continuously perfused with oxygenated artificial CSF (aCSF) maintained at 30°C using a solution heater (TC-324C, Warner Instruments, USA).

The spontaneous excitatory postsynaptic currents (sEPSC) were recorded in voltage-clamp mode at a holding potential of -70 mV. The sEPSC baseline was recorded 5 min after breaking in. An LED fiber above the recording sites emits blue (473 nm) light to activate the terminals of the eLPB^{ChAT} neurons within the lCeA or ovBNST. Mecamylamine (MEC, 5 μM, nicotinic actelycholine receptors antagonist) was used to non-specifically inhibit nicotinic acetylcholine receptors (nAChRs) [24].

All signals were filtered at 4 kHz, amplified at 5× using a MultiClamp 700B amplifier (Molecular Devices, USA) and digitized at 10 kHz with a Digidata 1550B analog-to-digital converter (Molecular Devices, USA). All data were analyzed with Clampfit 10.7 software (Molecular Devices, USA).

Elevated plus maze (EPM)

In the EPM experiment, male mice were assigned to receive a daily intraperitoneal injection of METH (METH group, 3 mg/kg) or saline (SAL group, 0.2 ml) for 7 consecutive days, followed by a 14-day abstinence (prolonged abstinence) period. On day 22, the EPM was performed to examine anxiety-like behaviors in male mice. The EPM apparatus (TopScan, USA) is composed of 4 elevated arms (52 cm above the floor) arranged in a cross pattern with two 1-cm walled arms (open arms) and two 40-cm walled arms (closed arms). Each male mouse was placed in the center portion of the EPM with its head directed towards an open arm, and allowed to freely explore the maze for 5 min. The time spent in and the entries into the open arms, as well as the total distance traveled within the apparatus were recorded and analyzed using TopScan H system (TopScan, USA).

For chemical genetics stimulations of the eLPB^{ChAT} terminals within the lCeA, the *rAAV2/9-ChAT-hM4D(Gi)-mCherry* (PT-3108, 6.28E+12 vg/ml, BrainVTA, China) virus was bilaterally injected into the eLPB (AP ± 5.19 mm, ML ± 1.45 mm, DV - 3.30 mm), and stainless-steel guide cannulas (O.D. 0.41 mm, C.C 4.0 mm, Cat 62004, RWD, China) were lowed into the lCeA (AP - 1.31 mm, ML ± 2.90 mm, DV - 4.50 mm). The guide cannulas were secured in place using glass ionomer cements. Dummy cannulas (62102, RWD, China, with lengths matching the guide cannulas) were placed inside the guide cannulas to prevent occlusion. Incisions were fixed and covered with glass ionomer cement.

Conditioned place preference (CPP)

The CPP test was performed in the TopScan3D CPP apparatus (CleverSys, USA), consisting of two distinct chambers (15 × 15 × 23 cm each) with a removable guillotine door. The CPP procedure involved a conditioning test (Pre-test, Day -1), conditioning (CPP training, Day 0-6), post-conditioning test (Test, Day 7), extinction training, and a saline or METH challenge-primed reinstatement test. Baseline preference (pre-test) was determined by allowing male mice to freely explore both chambers of the CPP apparatus for 15 min. Conditioning was conducted in a non-drug-paired chamber paired with a saline (0.2 ml, i.p.) injection in the morning and in a drug-paired chamber paired with a METH (3 mg/kg, i.p.) injection in the afternoon for 7 consecutive days. Following each injection, the male mice were confined to one chamber (non-drug-paired chamber or drug-paired chamber) for 45 min. During the test and extinction phases, male mice had unrestricted access to both chambers without any drug treatment. For the METH-primed reinstatement test, male mice received a subthreshold does of METH (0.5 mg/kg, i.p.) and were then allowed to freely explore both chambers for 15 min. The CPP score represents the time spent in drug-paired chamber minus that in the non-drug-paired chamber, while the ΔCPP score is calculated as the priming CPP score minus extinction CPP score.

In the chemical genetics stimulations experiment, the *rAAV2/9-ChAT-hM3D(Gq)-mCherry* (PT-2213, 5.54E+12 vg/ml, BrainVTA, China) or *rAAV2/9-ChAT-hM4D(Gi)-mCherry* (PT-3108, 6.28E+12 vg/ml, BrainVTA, China) virus was bilaterally injected into the eLPB (AP ± 5.19 mm, ML ± 1.45 mm, DV - 3.30 mm), and the cannulas were lowed into the lCeA (AP - 1.31 mm, ML ± 2.90 mm, DV – 3.0 mm) (cannula: O.D. 0.41 mm, C 4.0 mm, Cat 62004, RWD, China) or ovBNST (AP + 0.13 mm, ML ± 2.13

mm, DV - 2.62 mm, 15°tilt) (cannula: O.D. 0.41 mm, C 3.6 mm, Cat 62004, RWD, China).

Designer receptors exclusively activated by designer drugs (DREADDs)

Male mice were anesthetized with 2% isoflurane in oxygen and were fixed in a stereotactic frame (RWD, China). A heating pad was used to maintain the core body temperature of the animals at 37°C. 100 nl *rAAV2/9-ChAT-hM3D(Gq)-mCherry* (PT-2213, 5.54E+12 vg/ml, BrainVTA, China) or *rAAV2/9-ChAT-hM4D(Gi)-mCherry* (PT-3108, 6.28E+12 vg/ml, BrainVTA, China) virus was bilaterally injected into the eLPB (AP ± 5.19 mm, ML ± 1.45 mm, DV - 3.30 mm) at a rate of 1 nl/sec. After surgery, mice were allowed to recover in their homecage for one week. 10 min before the behavioral assays, CNO or saline was locally infused through the cannula at a flow rate of 0.1 µl/min. The infusion cannulas (#62204, RWD, China) were connected via polyethylene tubing (#62329, RWD, China) to 10-µl microsyringes (GAOGE, China) mounted on a microinfusion pump (RWDR462, China). For the diffusion of the drug, the infusion cannulas were kept in place for 5 min before being replaced with dummy cannulas. Male mice were injected with saline (vehicle, 0.2 ml) or CNO (2 mg/kg) 10 min before each behavioral test.

Statistical analysis

Statistical analysis was carried out using GraphPad Prism 8.0.2 software. All data are presented as the Mean ± SD. The data were analyzed by unpaired *t*-tests or two-way analysis of variance (ANOVA) with Sidak's multiple comparisons which appropriate. All statistical significance was set as $p < 0.05$.

Results

Anatomical dissection and functional investigation of the eLPB^{ChAT}–lCeA$^{PKC\delta}$ and eLPB^{ChAT}–ovBNST$^{PKC\delta}$ pathways

We conducted separate retrograde and anterograde tracer experiments in different batches of mice in the current study. Consistent with our previous study [14], we observed a widespread distribution of ChAT$^+$ neurons in the eLPB^{ChAT} along the anterior-posterior brain axis in naïve mice (Figures 1A, 1B and 1C). Here, employing the anterograde (Figures 1D, 1E and 1F) and retrograde (Figures 1G and 1H) virus tracing, we found that eLPB^{ChAT} neurons predominantly projected to lateral portion of CeA (lCeA) and the oval portion of BNST (ovBNST). Furthermore, approximately 75% and 52% of eLPB^{ChAT} terminals were distributed around PKCδ-positive (PKCδ$^+$) neurons in lCeA and ovBNST respectively, forming the eLPB^{ChAT}–lCeA$^{PKC\delta}$ pathway and eLPB^{ChAT}–ovBNST$^{PKC\delta}$ pathway.

Since cholinergic neurons have the potential to act as interneurons for local regulation [25] or innervating other nuclei through long projections [26, 27] in the brain, we explored the physiological innervation of eLPB^{ChAT} neurons on PKCδ$^+$ neurons in lCeA and ovBNST. First, to observe the real-time Ach signals from eLPB^{ChAT} terminals within the lCeA and ovBNST, DREADDs method and fiber photometry were employed in male naïve mice (Figures 2A, 2B and S1A). As shown in Figure S1B, systemic administration of CNO efficiently activates eLPB^{ChAT} neurons. In parallel, the Ach release was significantly increased in lCeA from 15 to 40 min (Figure 2C), and in ovBNST at 35 min following CNO injection (Figure 2D) in free-moving male mice compared to vehicle controls. In another set of identical mouse models, we collected brain tissue at 35 min after CNO injection and found that both lCeA$^{PKC\delta}$ neurons (Figure 2E) and ovBNST$^{PKC\delta}$ neurons (Figure 2F) were evoked by activating eLPB^{ChAT} neurons, as indicated by increased c-Fos$^+$ PKCδ$^+$ neurons. To further characterize the potential postsynaptic elements involved in the eLPB^{ChAT}–lCeA/ovBNST pathway, we employed optogenetic activation strategies combined with patch-clamp recordings on acutely prepared slices (Figures 2G and 2H). Blue light (473 nm) was utilized to activate the eLPB^{ChAT} terminals within either lCeA or ovBNST. As shown in Figures 2I and 2J, the frequency of sEPSC in the lCeA and ovBNST neurons was increased when activating LPB^{ChAT} terminals. Inhibition of nAChRs with mecamylamine incubation during optogenetic activation of eLPB^{ChAT} terminals resulted in a blockade of the triggered sEPSC frequency in slices of lCeA and ovBNST. Notably, no significant differences were observed in the amplitude of sEPSC between the lCeA and ovBNST neurons throughout the entire process. Collectively, these findings suggest that eLPB^{ChAT} neurons positively modulate lCeA$^{PKC\delta}$ and ovBNST$^{PKC\delta}$ neurons, at least partially through synaptic elements of presynaptic Ach release and postsynaptic nAChRs.

Inhibiting eLPB^{ChAT}–lCeA$^{PKC\delta}$ pathway alleviates anxiety-like behaviors in METH-withdrawn male mice

The involvement of LPB–CeA and LPB–BNST pathways in anxiety has been previously reported [15, 16, 28, 29]. Here, mice were subjected to daily intraperitoneal injections of METH or saline for 7 consecutive days, followed by a 14-day withdrawal period. Anxiety-like behaviors were assessed using EPM on Day 22 (Figure 3A).

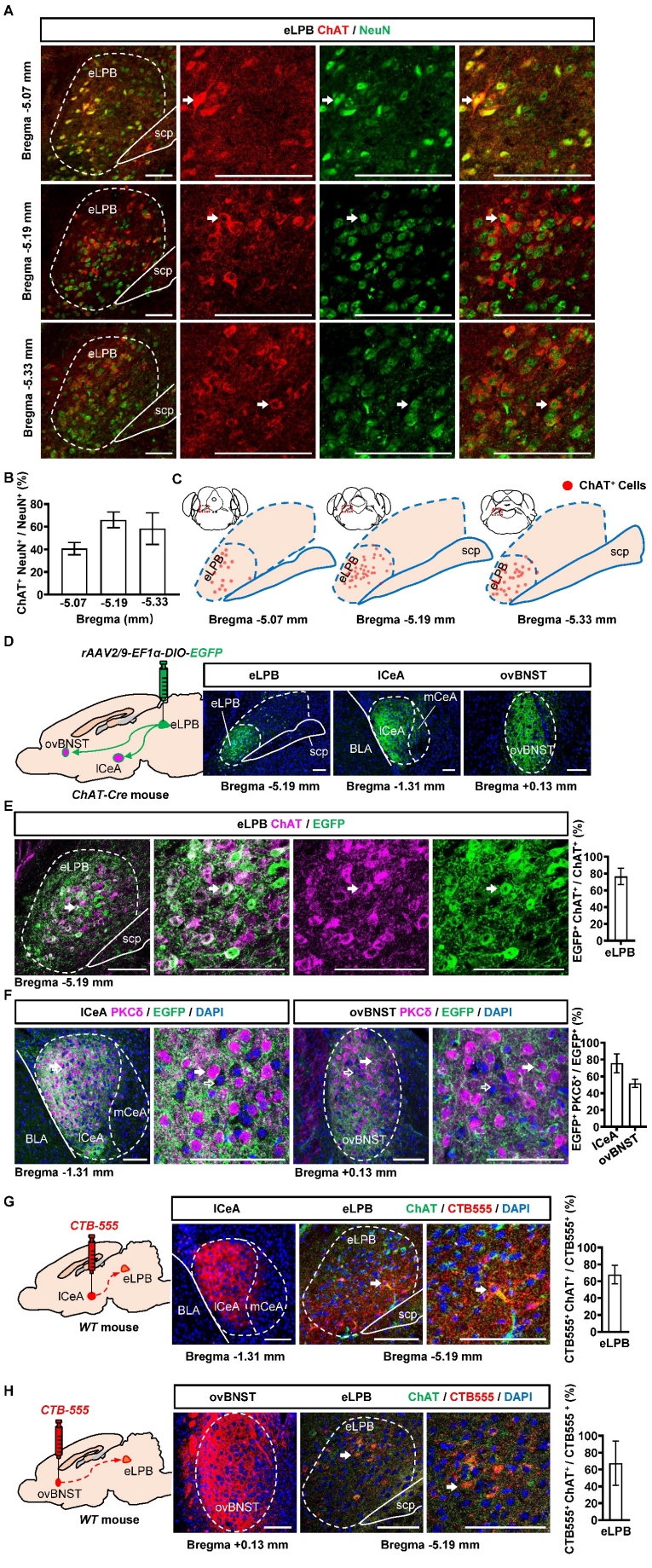

Figure 1. Anatomical structure of the eLPB^{ChAT}–lCeA^{PKCδ} and eLPB^{ChAT}–ovBNST^{PKCδ} pathways in naïve male mice. A, B Immunohistochemistry for ChAT/NeuN in the eLPB of WT mice. Scale bar, 100 μm. **C** Representative distribution images of ChAT neural ensemble in the eLPB. **D** Schematic diagram and representative images of the *rAAV2/9-DIO-EGFP* injection in the eLPB, lCeA and ovBNST in ChAT-Cre mouse. Scale bar, 100 μm. **E** Representative images and the percentage of EGFP-labelled neurons in the eLPB ChAT-positvie populations. Scale bar, 100 μm. **F** Representative images and the percentage of surrounded PKCδ-positive (PKCδ⁺) neurons in the lCeA and ovBNST. Scale bar, 100 μm. **G** Schematic diagram of the CTB-555 injection in the lCeA, the viral injection sites in the lCeA and CTB-555-labeled and ChAT that co-expressed within the eLPB of wild-type (WT) mouse. Scale bar, 100 μm. **H** Schematic diagram of the CTB-555 injection in the ovBNST, the viral injection sites in the ovBNST and CTB-555-labeled and ChAT that co-expressed within the eLPB of WT mouse. Scale bar, 100 μm.

In comparison with the saline-withdrawn mice, METH-withdrawn mice exhibited anxiety-like behaviors characterized by reduced time spent and fewer entries into the open arms (Figure 3B). Additionally, both eLPB^{ChAT} neurons and lCeA^{PKCδ} neurons, but not ovBNST^{PKCδ} neurons, showed significantly activation in METH-withdrawn male mice (Figure 3C).

To investigate the role of eLPB^{ChAT}–lCeA pathway in METH withdrawal-induced anxiety-like behavior, *rAAV2/9-ChAT-hM4D(Gi)-mCherry* virus was injected into the eLPB, and cannulas were placed in the lCeA. 10 min before EPM test, CNO or vehicle was locally infused through the cannula to selectively inhibit eLPB^{ChAT} terminals within the lCeA or not (Figures 4A and 4B). Results showed that inhibiting eLPB^{ChAT}–lCeA^{PKCδ} pathway decreased the activity of PKCδ⁺ neurons without affecting PKCδ⁻ neurons of the lCeA in both METH-withdrawn and control mice (Figure 4C). Additionally, inhibition of eLPB^{ChAT}–lCeA^{PKCδ} pathway efficiently attenuated anxiety-like behaviors specifically in METH-withdrawn male mice, while having no impact on related behaviors in controls (Figure 4D). Conversely, when we activated eLPB^{ChAT} terminals within the lCeA using similar viral tools (Figures 4E and 4F), there was an increased activation of PKCδ⁺ neurons but not PKCδ⁻ neurons in the lCeA (Figure 4G). As depicted in Figure 4H, activating eLPB^{ChAT}–lCeA^{PKCδ} pathway induced heightened anxiety-like behavior specifically in METH-withdrawn mice, while having no influence on such behavior in control mice.

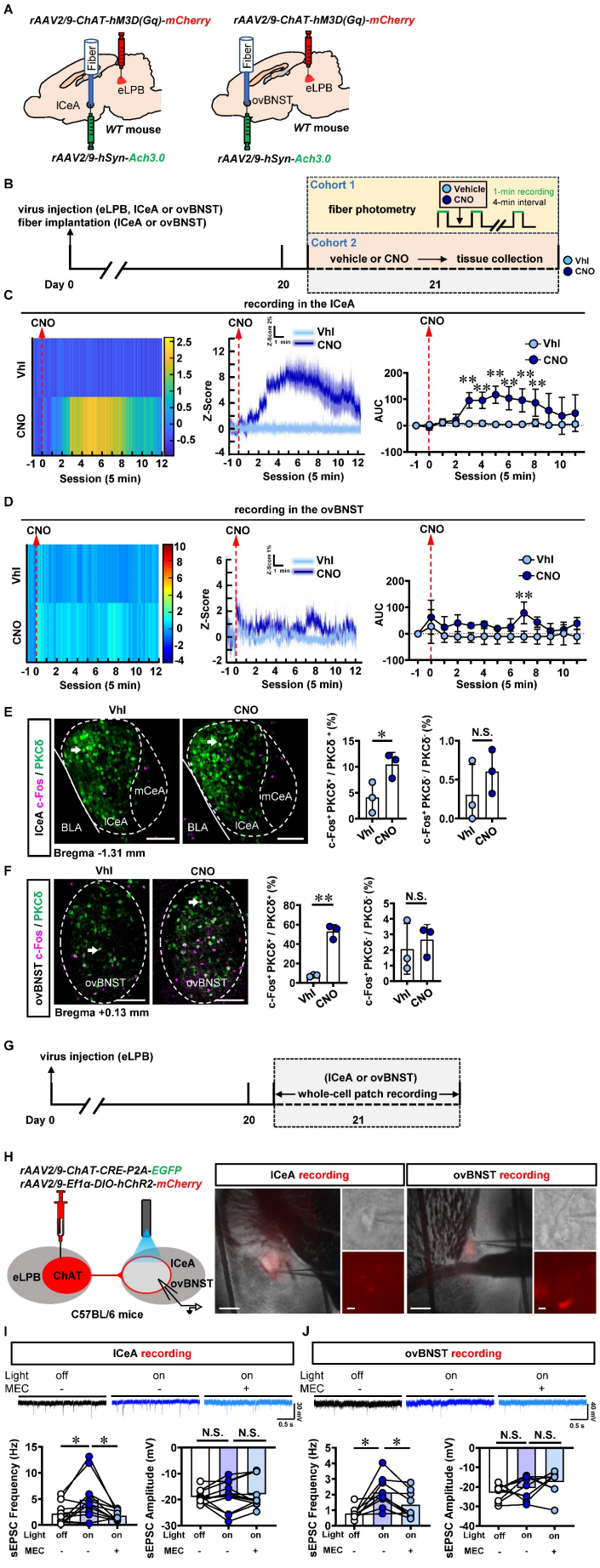

Figure 2. Functional innervation of the eLPB^{ChAT}–lCeA$^{PKC\delta}$ and eLPB^{ChAT}–ovBNST$^{PKC\delta}$ pathways in naïve male mice. A Schematic diagram of *rAAV2/9-ChAT-hM3D(Gq)-mCherry* injection into eLPB and fiber implantation in lCeA or ovBNST in WT mouse. **B** Experimental design and timeline in naïve male mice. **C** Heatmap (left), quantification (middle) and AUC (right) of Z-Score of Ach3.0 fluorescence in the lCeA. Two-way ANOVA with Sidak's multiple comparisons test. n = 5 mice per group. $F_{(12, 104)} = 4.730$, $p < 0.0001$; t = 4.545, *p (15 min) = 0.0002; t = 4.482, *p (20 min) = 0.0002; t = 5.780, **p (25 min) < 0.0001; t = 5.069, *p (30 min) < 0.0001; t = 4.675, *p (35 min) = 0.0001; t = 3.900, *p (40 min) = 0.0022. **D** Heatmap (left), quantification (middle) and AUC (right) of Z-Score of Ach3.0 fluorescence in the ovBNST. Two-way ANOVA with Sidak's multiple comparisons test. n = 3 mice per group. $F_{(12, 52)} = 0.7841$, $p = 0.6640$; t = 3.613, **p (35 min) = 0.0088. **E** The percentage of c-Fos-positive (c-Fos$^+$) neurons in the lCeA PKCδ$^+$ and PKCδ-negative (PKCδ$^-$) neurons. Two-tailed unpaired t test. n = 3 mice per group. c-Fos$^+$ PKCδ$^+$, $t_{(4)} = 2.925$, $p = 0.043$; c-Fos$^+$ PKCδ$^-$, $t_{(4)} = 1.076$, $p = 0.3426$. Scale bar, 100 μm. **F** The percentage of c-Fos$^+$ neurons in the ovBNST PKCδ$^+$ and PKCδ$^-$ neurons. Two-tailed unpaired t test. n = 3 mice per group. c-Fos$^+$ PKCδ$^+$, $t_{(4)} = 10.89$, $p = 0.0004$; c-Fos$^+$ PKCδ$^-$, $t_{(4)} = 0.5378$, $p = 0.6192$. Scale bar, 100 μm. **G** Experimental design and timeline of whole-cell path recording. **H** Schematic diagram of the viral transfection in mice and representative images of patch-clamp recording on the lCeA or ovBNST. Scale bar, 200 μm/5 μm. **I** Representative traces and statistics data of the lCeA neurons sEPSC. n = 12 cells from 6 mice. The one-way analysis of variance (ANOVA) with Tukey post-test. Frequency, $F_{(1.440, 15.84)} = 7.384$, $p = 0.0093$; *$p = 0.0316$ off vs on; *$p = 0.0365$ on vs on-MEC; Amplitude, $F_{(1.825, 20.07)} = 0.4156$, $p = 0.6473$; $p = 0.9690$ off vs on; $p = 0.7725$ on vs on-MEC. **J** Representative traces and statistics data of the ovBNST neurons sEPSC. n = 9 cells from 6 mice. The one-way analysis of variance (ANOVA) with Tukey post-test. Frequency, $F_{(1.486, 11.89)} = 9.790$, $p = 0.0049$; *$p = 0.0156$ off vs on; *$p = 0.0115$ on vs on-MEC; Amplitude, $F_{(1.859, 14.87)} = 2.762$, $p = 0.0983$; $p = 0.5846$ off vs on; $p = 0.4936$ on vs on-MEC. Vhl, vehicle; CNO, clozapine-N-oxide. *, $p < 0.05$, ** $p < 0.01$ vs Vhl.

Taken together, these findings suggest that the eLPB^{ChAT}–lCeA$^{PKC\delta}$ pathway is involved in encoding METH withdrawal anxiety, and has no influence on anxiety-like behavior in saline withdrawal mice.

Activating eLPB^{ChAT}–ovBNST$^{PKC\delta}$ pathway suppresses METH-primed reinstatement of CPP in male METH-exposed mice

Recently, emerging evidence demonstrate that PKCδ$^+$ GABAergic neurons might involve in encoding relapse to drugs [19, 30]. The METH-primed reinstatement of CPP procedure was established in male mice (Figure 5A). Our findings revealed that a single METH challenge (0.5 mg/kg) effectively induced the reinstatement of CPP in METH-exposed mice rather than those exposed to saline (Figures 5B and S2A). For the METH extinction mice, METH challenge resulted in heightened activity levels in eLPB^{ChAT}, lCeA$^{PKC\delta}$ and ovBNST$^{PKC\delta}$ neurons (Figure 5C). Further, METH priming induced a more pronounced increase in eLPB^{ChAT} and ovBNST$^{PKC\delta}$ neurons, with no discernible impact on lCeA$^{PKC\delta}$ neurons in METH-exposed mice compared to saline-exposed mice. These findings suggest that ovBNST$^{PKC\delta}$ neurons play a more prominent role in mediating METH-primed reinstatement of METH CPP.

Based on the neuronal activation phenotypes observed in METH-primed mice in the present

study, we speculate that precise inhibition of the eLPB^{ChAT}–lCeA$^{PKC\delta}$ or eLPB^{ChAT}–ovBNST$^{PKC\delta}$ pathway may attenuate the METH-primed reinstatement of CPP in METH-exposed mice. As shown in Figures 6A-6C, utilizing DREADDs methodology, we successfully achieved inhibition of eLPB^{ChAT} terminals in the lCeA$^{PKC\delta}$ in METH-exposed mice. Contrary to our initial expectations, inhibiting the eLPB^{ChAT}–lCeA$^{PKC\delta}$ pathway did not exert any influence on METH-primed reinstatement of CPP in mice (Figure 6D). Furthermore, there were no significant differences in ΔCPP score between the vehicle-treated and CNO-treated groups in saline-challenged METH-exposed mice (Figure 6D), suggesting that inhibiting eLPB^{ChAT} terminals in lCeA$^{PKC\delta}$ without administrating METH challenge cannot facilitate the reinstatement of CPP in mice. Previously, our research showed that activating eLPB^{ChAT} neurons or CeA–projecting eLPB^{ChAT} neurons, rather than suppressing them, could prevent METH-primed reinstatement of CPP in mice [14]. Therefore, we conducted local activation of eLPB^{ChAT} terminals in the lCeA$^{PKC\delta}$ in METH-exposed mice (Figures 6E and 6F). Unexpectedly, activating the eLPB^{ChAT}–lCeA$^{PKC\delta}$ pathway also failed to elicit any impact on METH-primed reinstatement of METH CPP in mice (Figure 6G), indicating that this pathway does not regulate METH-primed reinstatement behavior. These findings raise questions regarding other potential pathways involving eLPB^{ChAT} neurons responsible for modulating METH-primed reinstatement.

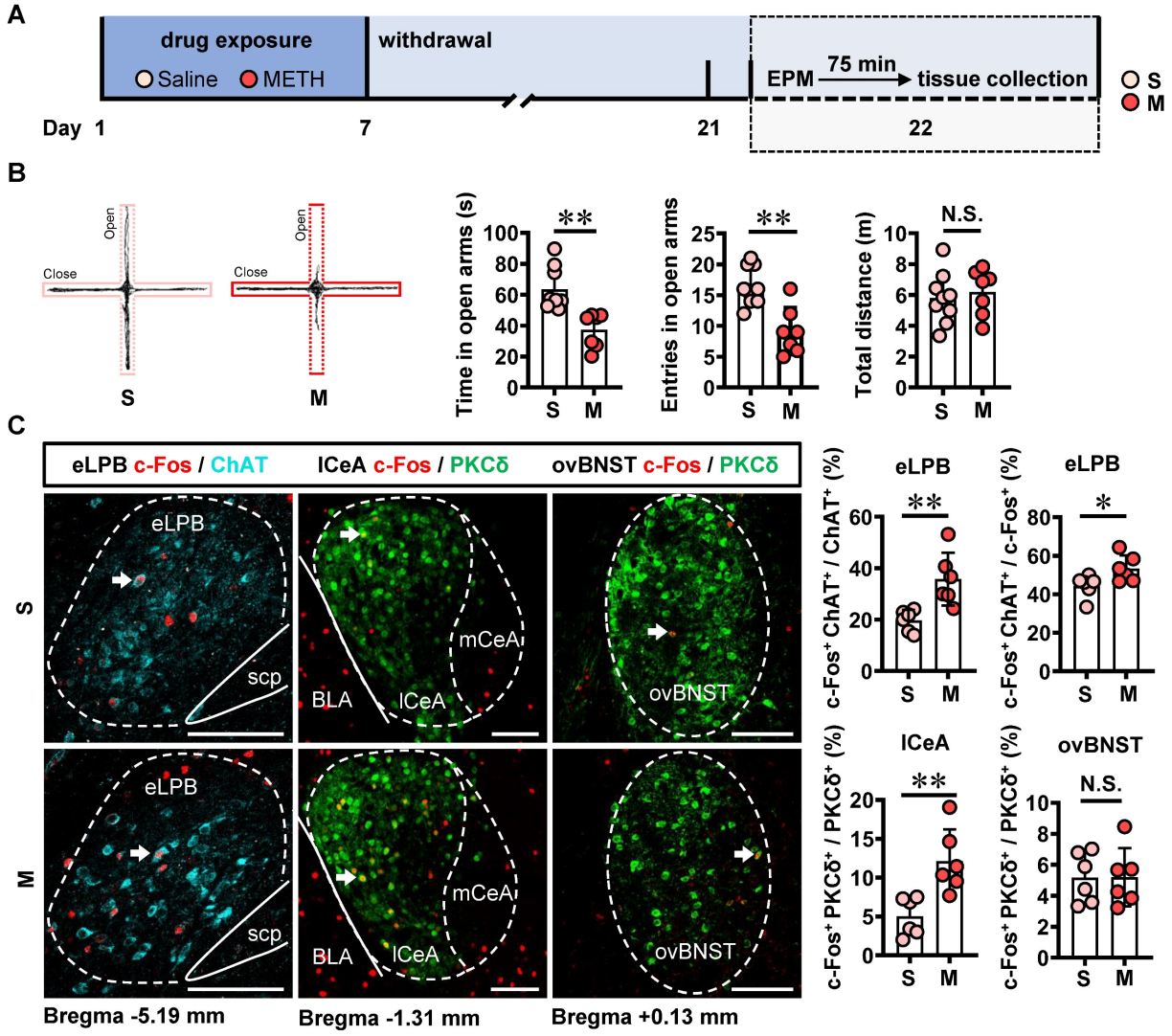

Figure 3. METH withdrawal enhances anxiety-like behaviors and triggers excitability of eLPB^{ChAT} and lCeA$^{PKC\delta}$ neurons in male mice. A Experimental design and timeline. **B** EPM test. Two-tailed unpaired t test. S group, n = 9 mice; M group, n = 7 mice. Time in open arms, $t_{(14)} = 4.060$, $p = 0.0012$. Entries into open arms, $t_{(14)} = 4.194$, $p = 0.0009$. Total distance, $t_{(14)} = 0.4946$, $p = 0.6285$. **C** Representative images and the percentage of c-Fos$^+$ neurons in the eLPB^{ChAT}, lCeA$^{PKC\delta}$ and ovBNST$^{PKC\delta}$ neurons. Two-tailed unpaired t test. n = 6 mice per group. eLPB (c-Fos$^+$ ChAT$^+$ / ChAT$^+$%), $t_{(10)} = 3.539$, $p = 0.0054$; eLPB (c-Fos$^+$ ChAT$^+$ / c-Fos$^+$%), $t_{(10)} = 2.413$, $p = 0.0365$; lCeA, $t_{(10)} = 3.636$, $p = 0.0046$; ovBNST, $t_{(10)} = 0.02581$, $p = 0.9799$.

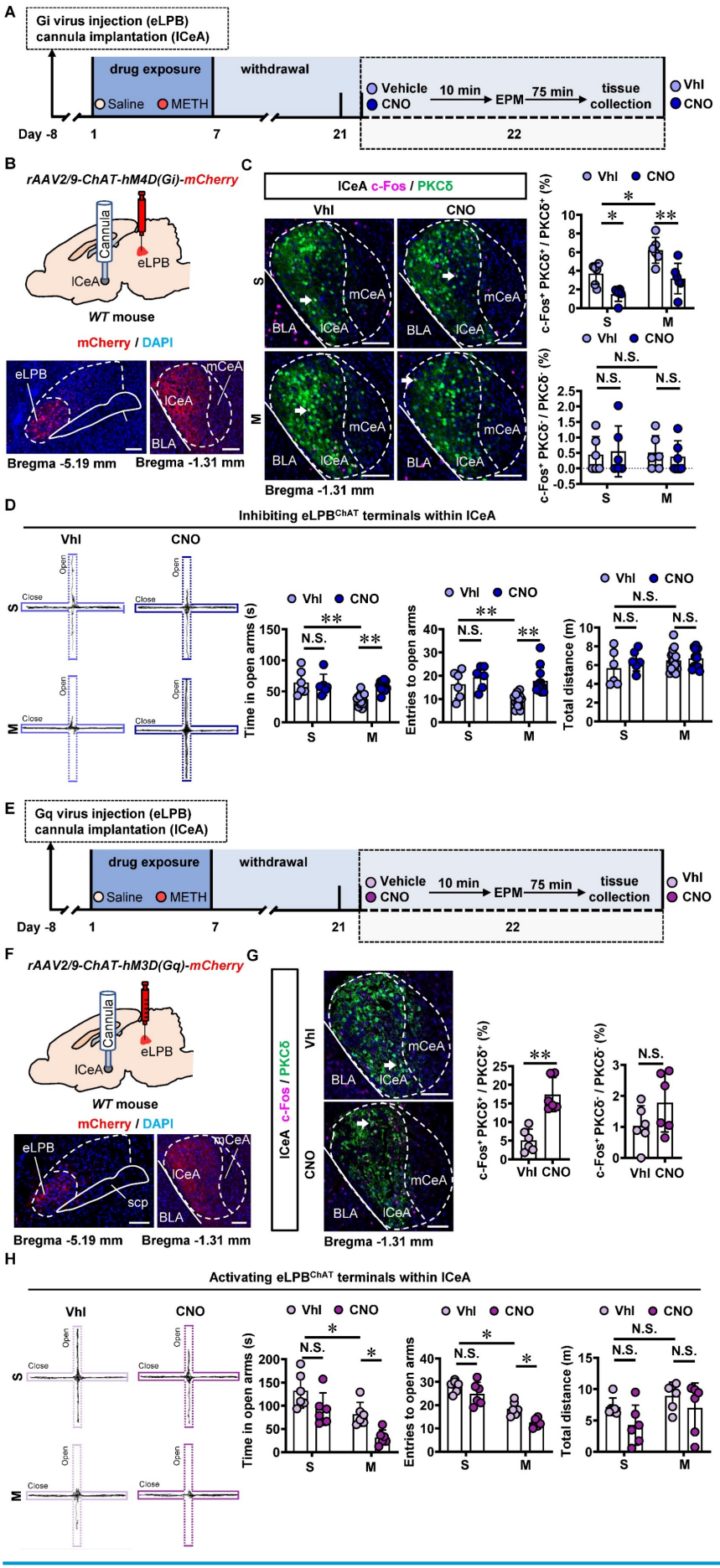

Figure 4. Inhibiting eLPB^{ChAT}–lCeA^{PKCδ} pathway alleviates the anxiety-like behaviors in METH-withdrawn male mice. A Experimental design and timeline of Gi virus in the eLPB. **B** Schematics and representative images of *rAAV2/9-ChAT-hM4D(Gi)-mCherry* injection in the eLPB, cannula implantation in the lCeA, and mCherry+ axon terminals in the lCeA of WT mouse. **C** Representative images and the percentage of c-Fos$^+$ neurons in the lCeA PKCδ$^+$ and PKCδ$^-$ neurons. Two-way ANOVA with Sidak's multiple comparisons test. Upper, n = 6 mice per group. $F_{(1, 20)} = 0.6286$, $p = 0.4372$; S-CNO group, t = 3.024, $p = 0.0395$ vs S-Vhl group; M-CNO group, t = 4.145, $p = 0.0030$ vs M-Vhl group; M-Vhl group, t = 3.405, $p = 0.0167$ vs S-Vhl group. Lower, n = 6 mice per group. $F_{(1, 20)} = 0.2019$, $p = 0.6580$; S-CNO group, t = 0.2862, $p = 0.9999$ vs S-Vhl group; M-CNO group, t = 0.3492, $p = 0.9996$ vs M-Vhl group; M-Vhl group, t = 0.1561, $p > 0.9999$ vs S-Vhl group. **D** EPM test. Two-way ANOVA with Sidak's multiple comparisons test. S-Vhl group, n = 6 mice; S-CNO group, n = 6 mice; M-Vhl group, n = 16 mice; M-CNO group, n = 12 mice. Time in open arms, $F_{(1, 36)} = 7.915$, $p = 0.0079$; S-CNO group, t = 0.5496, $p = 0.9950$ vs S-Vhl group; M-CNO group, t = 4.269, $p = 0.0008$ vs M-Vhl group; M-Vhl group, t = 4.552, $p = 0.0004$ vs S-Vhl group. Entries into open arms, $F_{(1, 36)} = 2.688$, $p = 0.1098$; S-CNO group, t = 1.132, $p = 0.8423$ vs S-Vhl group; M-CNO group, t = 4.684, $p = 0.0002$ vs M-Vhl group; M-Vhl group, t = 3.054, $p = 0.0251$ vs S-Vhl group. Total distance, $F_{(1, 36)} = 0.5195$, $p = 0.4757$; S-CNO group, t = 1.138, $p = 0.8395$ vs S-Vhl group; M-CNO group, t = 0.4135, $p = 0.9990$ vs M-Vhl group; M-Vhl group, t = 1.446, $p = 0.6409$ vs S-Vhl group. **E** Experimental design and timeline of Gq virus in the eLPB. **F** Schematics and representative images of *rAAV2/9-ChAT-hM3D(Gq)-mCherry* injection in the eLPB, cannula implantation in the lCeA, and mCherry+ axon terminals in the lCeA of WT mouse. **G** Representative images and the percentage of the percentage of c-Fos$^+$ neurons in and lCeA PKCδ$^+$ and PKCδ$^-$ neurons. Two-tailed unpaired t test. n = 6 mice per group. c-Fos$^+$ PKCδ$^+$ / PKCδ$^+$, $t_{(10)} = 5.514$, $p = 0.0003$; c-Fos$^+$ PKCδ$^-$ / PKCδ$^-$, $t_{(10)} = 1.595$, $p = 0.1417$. **H** EPM test. Two-way ANOVA with Sidak's multiple comparisons test. n = 6 mice per group. Time in open arms, $F_{(1, 20)} = 0.1872$, $p = 0.6699$; S-CNO group, t = 2.313, $p = 0.1745$ vs S-Vhl group; M-CNO group, t = 2.925, $p = 0.0492$ vs M-Vhl group; M-Vhl group, t = 2.957, $p = 0.0458$ vs S-Vhl group. Entries in open arms, $F_{(1, 20)} = 0.9668$, $p = 0.3372$; S-CNO group, t = 1.738, $p = 0.4599$ vs S-Vhl group; M-CNO group, t = 3.129, $p = 0.0313$ vs M-Vhl group; M-Vhl group, t = 5.041, t = 0.0004 vs S-Vhl group. Total distance, $F_{(1, 20)} = 0.1705$, $p = 0.6841$; S-CNO group, t = 1.764, $p = 0.4430$ vs S-Vhl group; M-CNO group, t = 1.180, $p = 0.8244$ vs M-Vhl group; M-Vhl group, t = 1.063, $p = 0.8827$ vs S-Vhl group. Vhl, vehicle; CNO, clozapine-N-oxide; S, saline; M, methamphetamine; N.S., $p > 0.05$, *, $p < 0.05$, **, $p < 0.01$ vs S or Vhl or CNO. Scale bar, 100 μm.

Similarly, we conducted inhibition of eLPB^{ChAT} terminals in the ovBNST^{PKCδ} in METH-exposed mice (Figures 7A, 7B and 7C). Consistent with the findings of eLPB^{ChAT}–lCeA^{PKCδ}, inhibiting the eLPB^{ChAT}–ovBNST^{PKCδ} pathway also had no influence on METH-primed reinstatement of CPP in mice (Figure 7D). Subsequently, we locally activated eLPB^{ChAT} terminals in the ovBNST^{PKCδ} in METH-exposed mice (Figures 7E and 7F), and found that activating eLPB^{ChAT}–ovBNST^{PKCδ} pathway effectively blocked

METH-primed reinstatement of METH CPP in mice (Figure 7G). We thought that the activation of eLPB^{ChAT} neurons by METH priming may represent a compensatory response of the brain, potentially attenuating sensitivity to drug priming by activating ovBNST$^{PKC\delta}$ neurons.

Taken together, these findings demonstrate that the eLPB^{ChAT}–ovBNST$^{PKC\delta}$ pathway, rather than eLPB^{ChAT}–CeA$^{PKC\delta}$ pathway, is encoding the METH-primed reinstatement of CPP.

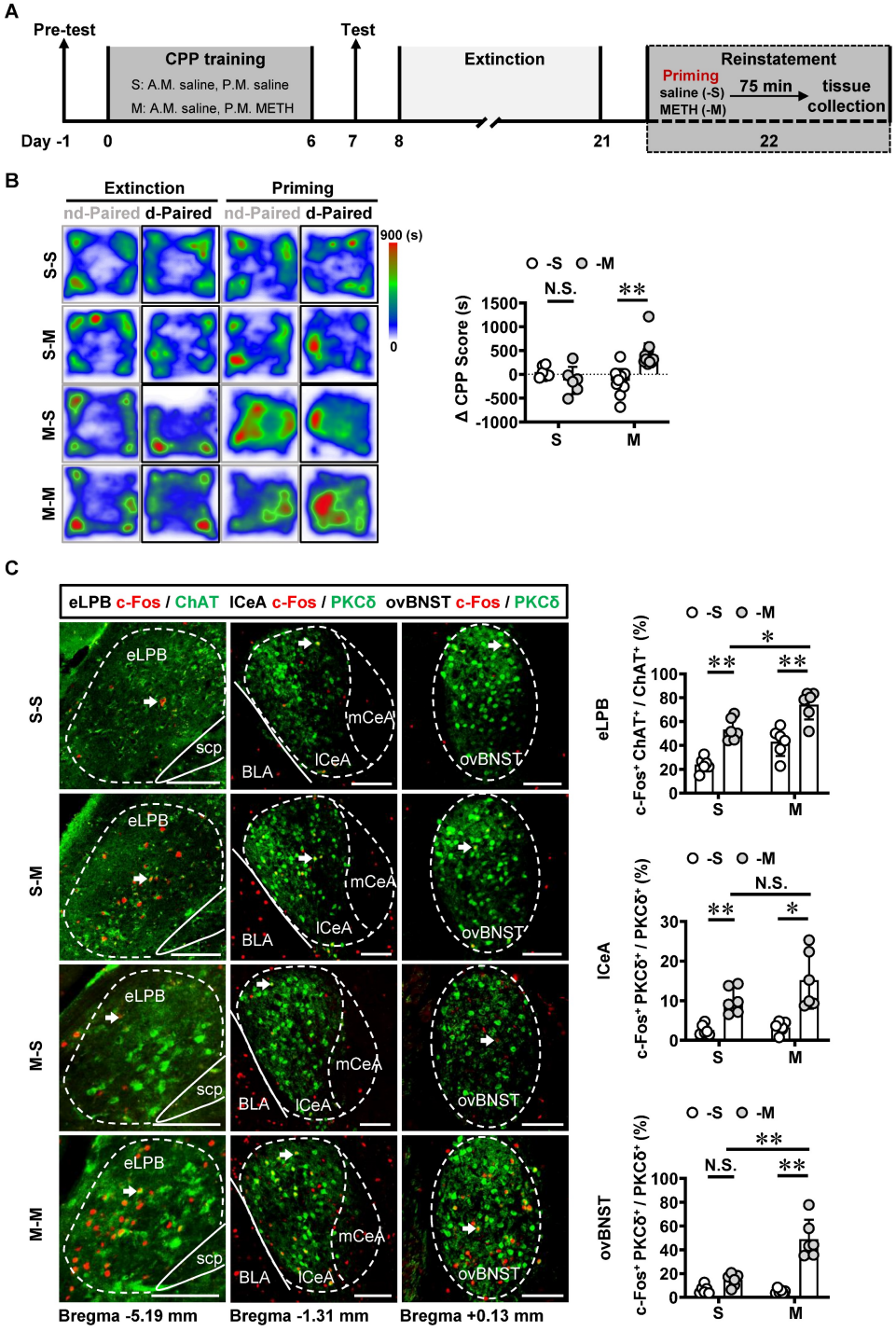

Figure 5. METH-primed reinstatement of CPP triggers excitability of the eLPB^{ChAT}, ICeA$^{PKC\delta}$ and ovBNST$^{PKC\delta}$ neurons in male mice. A Experimental design and timeline. **B** Heatmap of spent duration by mice in CPP apparatus and ΔCPP score. Two-way ANOVA with Sidak's multiple comparisons test. S group, n = 6 mice per group; M group, n = 14 mice per group. $F_{(1, 36)} = 18.16$, $p = 0.0001$; S-M group, t = 1.267, $p = 0.7630$ vs S-S group; M-M group, t = 5.846, $p < 0.0001$ vs M-S group. **C** Representative images and the percentage of c-Fos$^+$ neurons in the eLPB^{ChAT}, ICeA$^{PKC\delta}$ and ovBNST$^{PKC\delta}$ neurons. Two-way ANOVA with Sidak's multiple comparisons test. n = 6 mice per group. eLPB, $F_{(1, 20)} = 0.04656$, $p = 0.8313$; S-M group, t = 4.967, $p = 0.0004$ vs S-S group; M-M group, t = 5.272, $p = 0.0002$ vs M-S group; M-M group, t = 3.527, $p = 0.0126$ vs S-M group. ICeA, $F_{(1, 20)} = 1.737$, $p = 0.2024$; S-M group, t = 3.183, $p = 0.0277$ vs S-S group; M-M group, t = 5.047, $p = 0.0004$ vs M-S group; M-M group, t = 2.149, $p = 0.2367$ vs S-M group. ovBNST, $F_{(1, 20)} = 24.78$, $p < 0.0001$; S-M group, t = 1.587, $p = 0.5608$ vs S-S group; M-M group, t = 8.627, $p < 0.0001$ vs M-S group; M-M group, t = 6.764, $p < 0.0001$ vs S-M group. Scale bar, 100 μm. N.S., $p > 0.05$, *, $p < 0.05$, **, $p < 0.01$ vs S-S or M-S or Vhl or CNO.

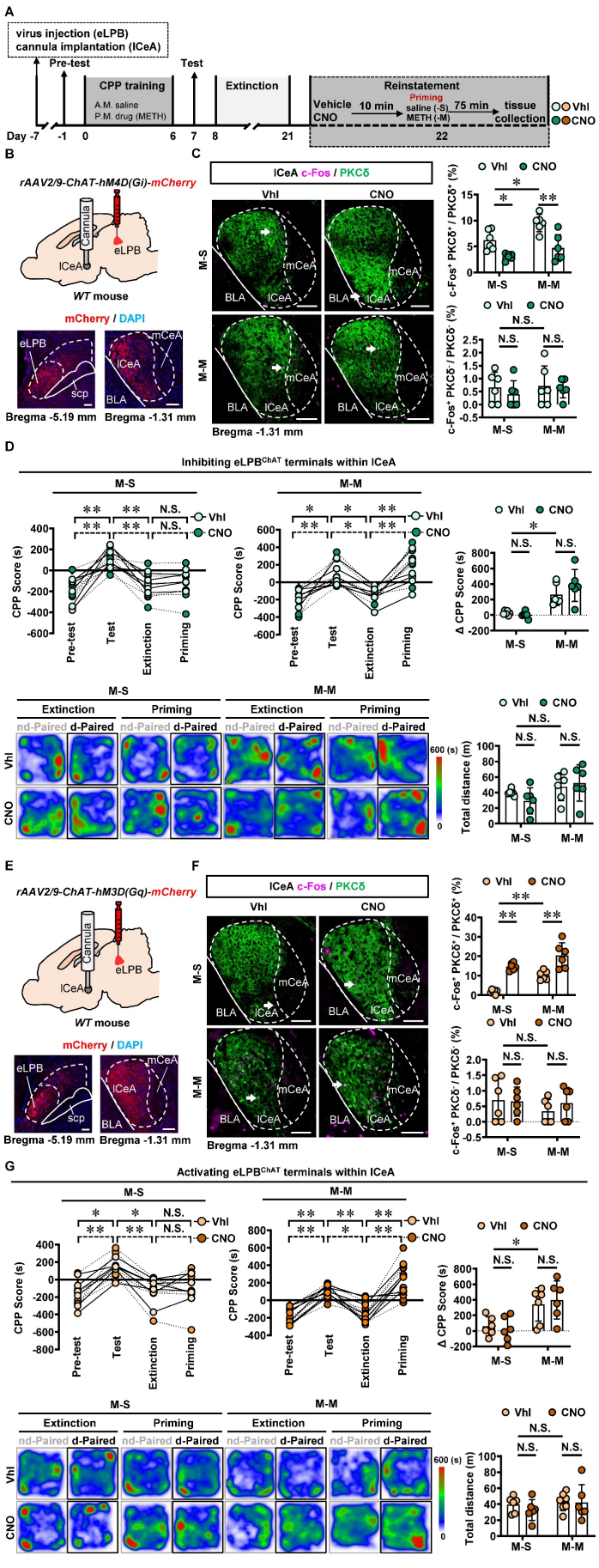

Figure 6. Manipulation of eLPB^{ChAT}–lCeA^{PKCδ} pathway had no influence on METH-primed reinstatement of CPP in mice. A Experimental design and timeline. **B** Schematics and representative images of *rAAV2/9-ChAT-hM4D(Gi)-mCherry* injection in the eLPB, cannula implantation into the lCeA, and mCherry+ axon terminals in the lCeA of WT mouse. **C** Representative images and the percentage of c-Fos+ neurons in PKCδ+ and PKCδ- neurons of lCeA. Two-way ANOVA with Sidak's multiple comparisons test. Upper, n = 6 mice per group. $F_{(1, 20)} = 1.300$, $p = 0.2676$; M-S-CNO group, t = 2.956, $p = 0.0459$ vs M-S-Vhl group; M-M-CNO group, t = 4.569, $p = 0.0011$ vs M-M-Vhl group; M-M-Vhl group, t = 3.141, $p = 0.0305$ vs M-S-Vhl group. Lower, n = 6 mice per group. $F_{(1, 20)} = 0.1319$, $p = 0.7203$; M-S-CNO group, t = 0.8018, $p = 0.9664$ vs M-S-Vhl group; M-M-CNO group, t = 0.2883, $p = 0.9999$ vs M-M-Vhl group; M-M-Vhl group, t = 0.1643, $p > 0.9999$ vs M-S-Vhl group. Scale bar, 100 μm. **D** CPP scores during the pre-test, CPP test, extinction and priming in M-S and M-M group and ΔCPP score (priming CPP score minus extinction CPP score). Two-way ANOVA with Sidak's multiple comparisons test. CPP scores, M-S group, n = 6 mice per group. $F_{(3, 40)} = 0.2925$, $p = 0.8305$; M-S-Vhl group priming, t = 0.3979, $p = 0.9992$ vs extinction; M-S-CNO group priming, t = 0.03663, $p > 0.9999$ vs extinction; M-M group, n = 6 mice per group. $F_{(3, 40)} = 0.9096$, $p = 0.4450$; M-M-Vhl group priming, t = 3.380, $p = 0.0097$ vs extinction; M-M-CNO group priming, t = 4.884, $p = 0.0001$ vs extinction. ΔCPP score, n = 6 mice per group. $F_{(1, 20)} = 1.919$, $p = 0.1812$; M-S-CNO group, t = 0.3304, $p = 0.9997$ vs M-S-Vhl group; M-M-CNO group, t = 1.629, $p = 0.5324$ vs M-M-Vhl group; M-M-Vhl group, t = 3.224, $p = 0.0253$ vs M-S-Vhl group. Heatmap of spent duration by mice in CPP apparatus and total distance traveled in CPP apparatus during priming test. Two-way ANOVA with Sidak's multiple comparisons test. n = 6 mice per group. $F_{(1, 20)} = 1.169$, $p = 0.2924$; M-S-CNO group, t = 1.068, $p = 0.8805$ vs M-S-Vhl group; M-M-CNO group, t = 0.4610, $p = 0.9982$ vs M-M-Vhl group; M-M-Vhl group, t = 0.7778, $p = 0.9710$ vs M-S-Vhl group. **E** Schematics and representative images of *rAAV2/9-ChAT-hM3D(Gq)-mCherry* injection in the eLPB, cannula implantation into the lCeA, and mCherry+ axon terminals in the lCeA of WT mouse. **F** Representative images and the percentage of c-Fos+ neurons in the lCeA PKCδ+ and PKCδ- neurons. Two-way ANOVA with Sidak's multiple comparisons test. Upper, n = 6 mice per group. $F_{(1, 20)} = 0.7879$, $p = 0.3853$; M-S-CNO group, t = 6.110, $p < 0.0001$ vs M-S-Vhl group; M-M-CNO group, t = 4.855, $p = 0.0006$ vs M-M-Vhl group; M-M-Vhl group, t = 3.940, $p = 0.0048$ vs M-S-Vhl group. Lower, n = 6 mice per group. $F_{(1, 20)} = 0.5010$, $p = 0.4872$; M-S-CNO group, t = 0.1483, $p > 0.9999$ vs M-S-Vhl group; M-M-CNO group, t = 0.8527, $p = 0.9552$ vs M-M-Vhl group; M-M-Vhl group, t = 1.181, $p = 0.8242$ vs M-S-Vhl group. Scale bar, 100 μm. **G** CPP scores during the pre-test, CPP test, extinction and priming in M-S and M-M group and ΔCPP score. Two-way ANOVA with Sidak's multiple comparisons test. CPP scores, M-S-Vhl, n = 6 mice; M-S-CNO group, n = 6 mice; M-M-Vhl group, n = 7 mice; M-M-CNO group, n = 6 mice; M-S group, $F_{(3, 40)} = 0.2600$, $p = 0.8537$; M-S-Vhl group priming, t = 0.6514, $p = 0.9875$ vs extinction; M-S-CNO group priming, t = 0.2366, $p > 0.9999$ vs extinction; M-M group, $F_{(3, 44)} = 0.1465$, $p = 0.9314$; M-M-Vhl group priming, t = 5.055, $p < 0.0001$ vs extinction; M-M-CNO group priming, t = 5.445, $p < 0.0001$ vs extinction. ΔCPP score, M-S-Vhl group, n = 6 mice; M-S-CNO group, n = 6 mice; M-M-Vhl group, n = 7 mice. M-S-CNO group, n = 6 mice. $F_{(1, 21)} = 0.3640$, $p = 0.5528$; M-S-CNO group, t = 0.3362, $p = 0.9997$ vs M-S-Vhl group; M-M-CNO group, t = 0.5205, $p = 0.9964$ vs M-M-Vhl group; M-M-Vhl group, t = 2.633, $p = 0.0894$ vs M-S-Vhl group. Heatmap of spent duration by mice in CPP apparatus and total distance traveled in CPP apparatus during priming test. Two-way ANOVA with Sidak's multiple comparisons test. M-S-Vhl group, n = 6 mice; M-S-CNO group, n = 6 mice; M-M-Vhl group, n = 7 mice; M-S-CNO group, n = 6 mice. $F_{(1, 21)} = 0.2734$, $p = 0.6066$; M-S-CNO group, t = 0.8464, $p = 0.9565$ vs M-S-Vhl group; M-M-CNO group, t = 0.1249, $p > 0.9999$ vs M-M-Vhl group; M-M-Vhl group, t = 0.4007, $p = 0.9992$ vs M-S-Vhl group. Vhl, vehicle; CNO, clozapine-N-oxide; M-S, saline-primed reinstatement test following METH CPP extinction training; M-M, METH-primed reinstatement test following METH CPP extinction training; N.S., $p > 0.05$, *, $p < 0.05$, **, $p < 0.01$.

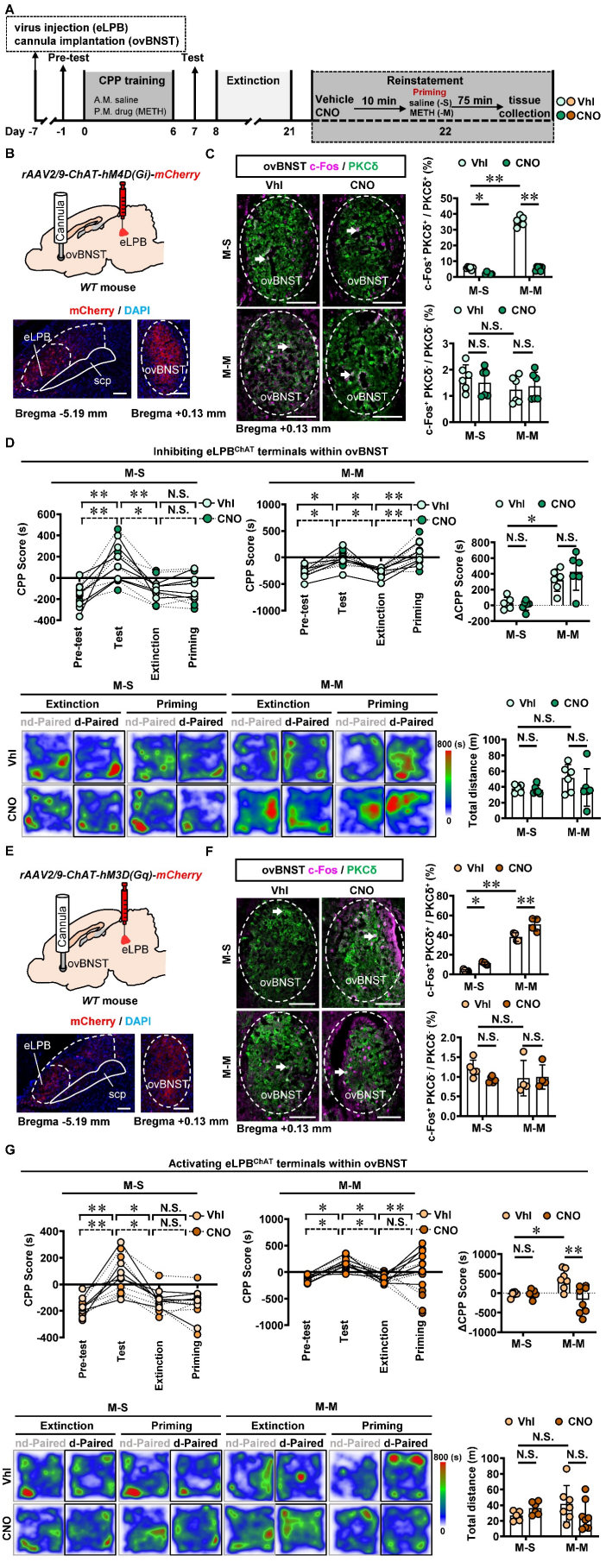

Figure 7. Activating eLPB^{ChAT}–ovBNST^{PKCδ} pathway suppresses METH-primed reinstatement of CPP in male METH-exposed mice. A Experimental design and timeline. **B** Schematics and representative images of *rAAV2/9-ChAT-hM4D(Gi)-mCherry* injection in the eLPB, cannula implantation into the ovBNST, and mCherry+ axon terminals in the ovBNST of WT mouse. **C** Representative images and the percentage of c-Fos$^+$ neurons in PKCδ$^+$ and PKCδ$^-$ neurons of the ovBNST. Two-way ANOVA with Sidak's multiple comparisons test. Upper, n = 6 mice per group. $F_{(1, 20)} = 351.3$, $p < 0.0001$; M-S-CNO group, t = 3.564, $p = 0.0116$ vs M-S-Vhl group; M-M-CNO group, t = 30.07, $p < 0.0001$ vs M-M-Vhl group; M-M-Vhl group, t = 29.87, $p < 0.0001$ vs M-S-Vhl group. Lower, n = 6 mice per group. $F_{(1, 20)} = 0.6128$, $p = 0.4429$; M-S-CNO group, t = 0.6598, $p = 0.9873$ vs M-S-Vhl group; M-M-CNO group, t = 0.4473, $p = 0.9984$ vs M-M-Vhl group; M-M-Vhl group, t = 1.529, $p = 0.6009$ vs M-S-Vhl group. Scale bar, 100 μm. **D** CPP scores during the pre-test, CPP test, extinction and priming in M-S and M-M group and ΔCPP score. Two-way ANOVA with Sidak's multiple comparisons test. CPP scores, n = 6 mice per group. M-S group, $F_{(3, 40)} = 0.1050$, $p = 0.9567$; M-S-Vhl group priming, t = 0.3309, $p = 0.9997$ vs extinction; M-S-CNO group priming, t = 0.003933, $p > 0.9999$ vs extinction; M-M group, n = 6 mice per group. $F_{(3, 40)} = 0.3636$, $p = 0.7796$; M-M-Vhl group priming, t = 3.698, $p = 0.0039$ vs extinction; M-M-CNO group priming, t = 4.924, $p < 0.0001$ vs extinction. ΔCPP score, n = 6 mice per group. $F_{(1, 20)} = 1.261$, $p = 0.2748$; M-S-CNO group, t = 0.3214, $p = 0.9998$ vs M-S-Vhl group; M-M-CNO group, t = 1.267, $p = 0.7745$ vs M-M-Vhl group; M-M-Vhl group, t = 3.502, $p = 0.0134$ vs M-S-Vhl group. Heatmap of spent duration by mice in CPP apparatus and total distance traveled in CPP apparatus during priming test. Two-way ANOVA with Sidak's multiple comparisons test. n = 6 mice per group. $F_{(1, 20)} = 0.6880$, $p = 0.4167$; M-S-CNO group, t = 0.2092, $p > 0.9999$ vs M-S-Vhl group; M-M-CNO group, t = 1.382, $p = 0.7007$ vs M-M-Vhl group; M-M-Vhl group, t = 1.515, $p = 0.6106$ vs M-S-Vhl group. **E** Schematics and representative images of *rAAV2/9-ChAT-hM3D(Gq)-mCherry* injection in the eLPB, cannula implantation in the ovBNST, and mCherry+ axon terminals in the ovBNST of WT mouse. **F** Representative images and the percentage of c-Fos$^+$ neurons in the ovBNST PKCδ$^+$ and PKCδ$^-$ neurons. Two-way ANOVA with Sidak's multiple comparisons test. Upper, M-S group, n = 5 mice per group; M-M group, n = 4 mice per group. $F_{(1, 14)} = 2.226$, $p = 0.1579$; M-S-CNO group, t = 3.091, $p = 0.0469$ vs M-S-Vhl group; M-M-CNO group, t = 4.766, $p = 0.0018$ vs M-M-Vhl group; M-M-Vhl group, t = 13.42, $p < 0.0001$ vs M-S-Vhl group. Lower, M-S group, n = 5 mice per group; M-M group, n = 4 mice per group. $F_{(1, 14)} = 1.312$, $p = 0.2713$; M-S-CNO group, t = 1.562, $p = 0.5972$ vs M-S-Vhl group; M-M-CNO group, t = 0.1395, $p > 0.9999$ vs M-M-Vhl group; M-M-Vhl group, t = 1.270, $p = 0.7828$ vs M-S-Vhl group. Scale bar, 100 μm. **G** CPP scores during the pre-test, CPP test, extinction and priming in M-S and M-M group and ΔCPP score. Two-way ANOVA with Sidak's multiple comparisons test. CPP scores, M-S-Vhl group, n = 6 mice; M-S-CNO group, n = 6 mice; M-M-Vhl group, n = 7 mice; M-M-CNO group, n = 8 mice. M-S group, $F_{(3, 40)} = 0.08858$, $p = 0.9659$; M-S-Vhl group priming, t = 0.4327, $p = 0.9986$ vs extinction; M-S-CNO group priming, t = 0.1847, $p > 0.9999$ vs extinction; M-M group, $F_{(3, 52)} = 8.126$, $p = 0.0002$; M-M-Vhl group priming, t = 3.769, $p = 0.0025$ vs extinction; M-M-CNO group priming, t = 1.952, $p = 0.2937$ vs extinction. ΔCPP score, M-S-Vhl group, n = 6 mice; M-S-CNO group, n = 6 mice; M-M-Vhl group, n = 7 mice; M-M-CNO group, n = 8 mice. $F_{(1, 23)} = 8.648$, $p = 0.0073$; M-S-CNO group, t = 0.1133, $p > 0.9999$ vs M-S-Vhl group; M-M-CNO group, t = 4.279, $p = 0.0017$ vs M-M-Vhl group; M-M-Vhl group, t = 2.887, $p = 0.0489$ vs M-S-Vhl group. Heatmap of spent duration by mice in CPP apparatus and total distance traveled in CPP apparatus during priming test. Two-way ANOVA with Sidak's multiple comparisons test. M-S-Vhl group, n = 6 mice; M-S-CNO group, n = 6 mice; M-M-Vhl group, n = 7 mice; M-M-CNO group, n = 8 mice. $F_{(1, 23)} = 3.759$, $p = 0.0649$; M-S-CNO group, t = 0.9591, $p = 0.9228$ vs M-S-Vhl group; M-M-CNO group, t = 1.834, $p = 0.3919$ vs M-M-Vhl group; M-M-Vhl group, t = 1.623, $p = 0.5302$ vs M-S-Vhl group. Vhl, vehicle; CNO, clozapine-N-oxide; S-S, saline challenge-primed reinstatement test following saline CPP extinction training; S-M, METH challenge-primed reinstatement test following saline CPP extinction training; M-S, saline-primed reinstatement test following METH CPP extinction training; M-M, METH-primed reinstatement test following METH CPP extinction training; N.S., $p > 0.05$, *, $p < 0.05$, **, $p < 0.01$ vs S-S or M-S or Vhl or CNO.

Discussion

In summary, our study has made a novel discovery by identifying two distinct anatomically and functionally pathways of eLPB^{ChAT} neurons, namely eLPB^{ChAT}–lCeA$^{PKC\delta}$ pathway and eLPB^{ChAT}–ovBNST$^{PKC\delta}$ pathway. We further elucidate the involvement of synaptic elements of presynaptic Ach release and postsynaptic nAChRs in the positive innervation of the two cholinergic pathways. Importantly, our findings demonstrate that METH withdrawal anxiety and METH-primed reinstatement of CPP respectively recruit eLPB^{ChAT}–lCeA$^{PKC\delta}$ and eLPB^{ChAT}–ovBNST$^{PKC\delta}$ pathway in METH-exposed male mice (Figure 8).

In our previous study [14], chemogenetic activation of either the eLPB^{ChAT} neurons or the CeA-projecting eLPB^{ChAT} neurons significantly suppressed METH primed-reinstatement of CPP in mice. Here, our chemogenetic experiments specifically targeted the eLPB^{ChAT} projection to the lCeA using DREADD virus in the eLPB, followed by a site-specific infusion of the CNO into the lCeA to evaluate the effects of eLPB^{ChAT}–lCeA pathway in METH primed-reinstatement. We found that chemogenetic modulation of local presynaptic activity at eLPB^{ChAT} axon terminals within the eLPB^{ChAT}–lCeA pathway had no effect on METH primed-reinstatement of CPP. These seemingly contradictory findings raise significant concerns regarding whether eLPB^{ChAT} neurons projecting to other brain regions encode METH primed-reinstatement of CPP.

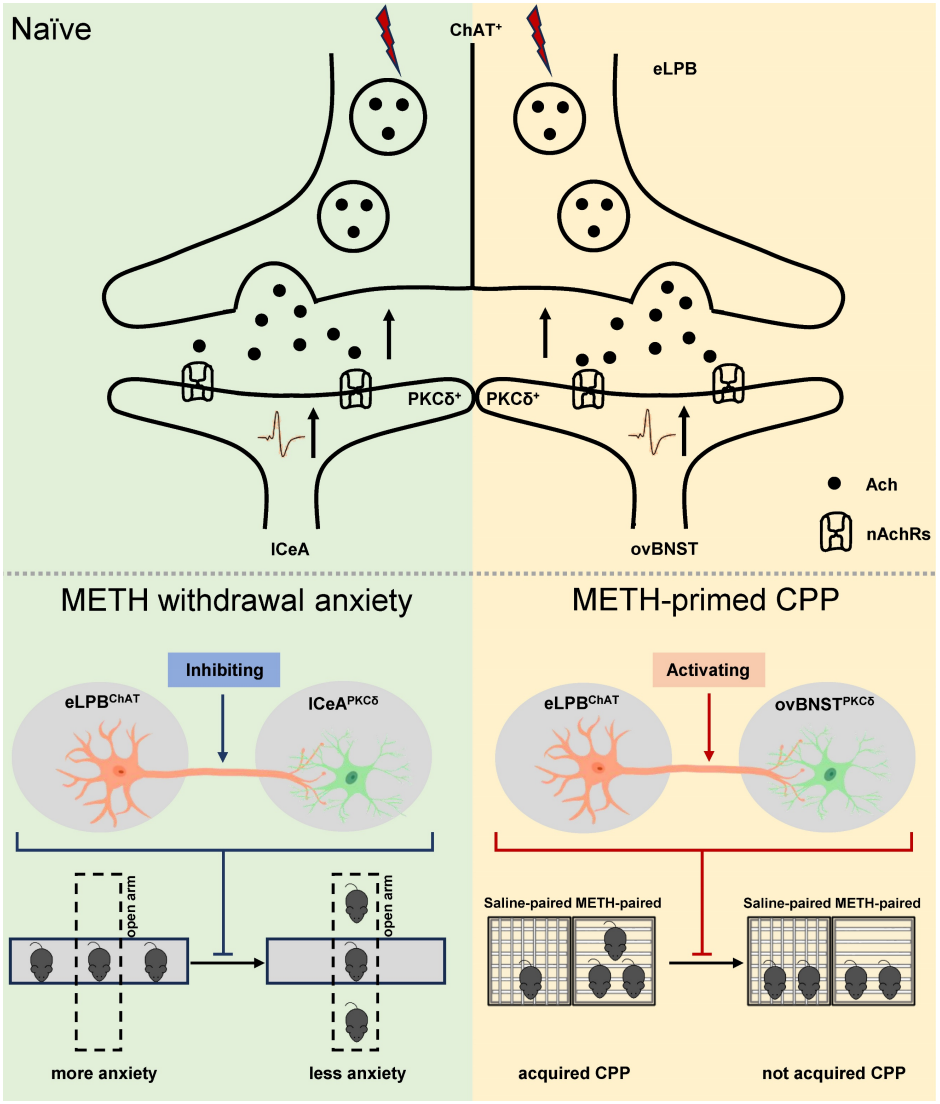

Figure 8. Schematic diagram of the present study. The ChAT$^+$ neurons in the eLPB send projections to PKCδ$^+$ neurons in the lCeA and ovBNST, forming eLPB^{ChAT}–lCeA$^{PKC\delta}$ and eLPB^{ChAT}–ovBNST$^{PKC\delta}$ pathways. At least in part, the eLPB^{ChAT} neurons positively excite the lCeA$^{PKC\delta}$ neurons and ovBNST$^{PKC\delta}$ neurons through synaptic elements of presynaptic Ach release and postsynaptic nAChRs. Chemogenetic inhibiting the eLPB^{ChAT} terminals within the lCeA alleviates the anxiety-like behaviors in METH-withdrawn mice, and chemogenetic activating the eLPB^{ChAT} terminals within the ovBNST blocks METH-primed reinstatement of CPP in METH-exposed mice. These results indicate that METH withdrawal anxiety and METH-primed relapse recruit distinct eLPB^{ChAT} projections, as identified by eLPB^{ChAT}–lCeA$^{PKC\delta}$ pathway and eLPB^{ChAT}–ovBNST$^{PKC\delta}$ pathway, respectively.

In addition to fMOST results [14], anterograde and retrograde tracing results in the present study also revealed an additional region of substantial innervation, namely ovBNST, which is in line with previous immunohistochemical studies [13, 31]. Convincing empirical support has substantiated the pivotal role of the BNST in facilitating stress-induced reinstatement of drug seeking [32-35]. For example, mimic α2a-adrenergic receptor [33] or activating pituitary adenylate cyclase-activating peptide (PACAP) systems [32] in the BNST was sufficient to induce reinstatement of cocaine. Notably, injections of the corticotropin releasing factor (CRF) receptor antagonist into the BNST attenuated stress-induced reinstatement of cocaine [36] and morphine [37] seeking, whereas no such effect was observed in the amygdala. However, the role of BNST and CeA in reinstatement of drug seeking is controversial, as conflicting findings have been reported in various studies. For example, injections of the CRF receptor antagonist into the amygdala, but not the BNST, attenuated morphine primed-reinstatement of CPP [37]. Furthermore, the blockade of noradrenergic receptors in both the BNST and the CeA effectively prevented stress-induced reinstatement of cocaine seeking, but did not influence cocaine primed-reinstatement [38]. Reversible tetrodotoxin (TTX) lesions of either the BNST or the CeA blocked stress-induced reinstatement of heroin seeking [35]. To data, the investigation of BNST and CeA, particularly those neurons receiving $eLPB^{ChAT}$ projections, has been sparsely documented in METH seeking. Here, our study presents the first evidence of the $eLPB^{ChAT}$–$lCeA^{PKC\delta}$ pathway and $eLPB^{ChAT}$–$ovBNST^{PKC\delta}$ pathway. Results showed that activating $eLPB^{ChAT}$–$ovBNST^{PKC\delta}$ pathway, but not the $eLPB^{ChAT}$–$lCeA^{PKC\delta}$ pathway, suppressed METH-primed reinstatement of CPP in male METH-exposed mice. In light of these findings, we wondered whether distinct outputs from the $eLPB^{ChAT}$ mediate different components of the METH-related behavior.

Studies indicated the CeA as a target for anxiolytic agents [39, 40]. The lCeA is often referred to as the "nociceptive amygdala" due to its high concentration of neurons that respond to noxious stimuli which receive nociceptive-specific information through the PBN [41, 42]. The lCeA predominantly consists of $PKC\delta^{+}$ neurons [43, 44], and optogenetic activation of $lCeA^{PKC\delta}$ was anxiolytic [45]. Additionally, LPB neurons projected to the lCeA, forming a functionally significant circuit involved in appetite suppression [31] and the formation of aversive memories [6]. A recent study demonstrated that chemogenetic stimulation of LPB–CeA pathway heightened anxiety-like behavior [13]. In this study, we found that inhibiting $eLPB^{ChAT}$–$lCeA^{PKC\delta}$ pathway alleviated anxiety-like behaviors in METH-withdrawn male mice, indicating the $eLPB^{ChAT}$ may serve as the primary source of $lCeA^{PKC\delta}$ relevant to METH withdrawal-induced anxiety-like behavior.

In the current study, we found that both $eLPB^{ChAT}$ and $ovBNST^{PKC\delta}$ neurons were activated following METH-primed reinstatement of CPP, while it was to activating rather than suppressing $eLPB^{ChAT}$–ovBNST pathway blocked METH-primed reinstatement of CPP in mice. We predict that the activation of this pathway may be a compensatory effect for the METH-primed reinstatement of METH CPP. Notably, $eLPB^{ChAT}$ neurons were activated as early as METH withdrawal period, while $ovBNST^{PKC\delta}$ neurons were activated after METH priming rather than the METH withdrawal period. Further, we found that activating $eLPB^{ChAT}$ neurons enhanced the Ach release within the ovBNST, as well as triggered $ovBNST^{PKC\delta}$ neurons in mice. As such, we suspect that the activation of $eLPB^{ChAT}$ neurons is a direct result of the concomitant effect with METH exposure, while the activation of $ovBNST^{PKC\delta}$ neurons might be secondary occurrence only after METH priming during the reinstatement of METH CPP. The BNST mainly consists of GABAergic neurons, which send inhibitory projections to some addition-related brain regions, such as ventral tegmental area [46] and nucleus accumbens [47]. Therefore, activating $eLPB^{ChAT}$–$ovBNST^{PKC\delta}$ pathway has potential to enhance the inhibitory outputs from ovBNST, which might inhibit these addiction-related regions and subsequently suppress the METH-primed reinstatement of CPP.

There are several limitations in the current study. First, there is lack of female mice models to explore the potential sex differences in the impact of $eLPB^{ChAT}$ projections on METH toxicity. Second, there is the absence of PKCδ-promoter-tagged viral tools or animal models, which hindered the precise manipulation of $CeA^{PKC\delta}$ or $BNST^{PKC\delta}$ neurons *in vivo*.

Conclusions

Collectively, our data show that the $eLPB^{ChAT}$ is a critical node in the neural networks governing METH withdrawal anxiety and METH primed-reinstatement of CPP through its projections to the $lCeA^{PKC\delta}$ and $ovBNST^{PKC\delta}$, respectively.

Abbreviations

Ach: acetylcholine; AUC: area under the curve; CeA: central nucleus of the amygdala; BNST: bed nucleus of the stria terminalis; $ChAT^{+}$: choline acetyltransferase; CNO: clozapine-N-oxide; CPP: conditioned place preference; CRF: corticotropin releasing factor; DREADDs: Designer receptors

exclusively activated by designer drugs; eLPB: external lateral portion of parabrachial nucleus; EPM: elevated plus maze; IACUC: Institutional Animal Care and Use Committee; lCeA: lateral portion of central nucleus of amygdala; MEC: Mecamylamine; METH: methamphetamine; MUD: METH use disorders; nAChRs: nicotinic acetylcholine receptors; ovBNST: oval portion of bed nucleus of the stria terminalis; PACAP: pituitary adenylate cyclase-activating peptide; PBN: parabrachial nucleus; PFA: paraformaldehyde; PKCδ: protein kinase C delta; sEPSC: spontaneous excitatory postsynaptic currents; TTX: tetrodotoxin; WT: wild type.

Supplementary Material

Supplementary figures.
https://www.thno.org/v14p2881s1.pdf

Acknowledgements

We thank Prof. Minmin Luo, National Institute of Biological Science, Beijing, China, for giving ChAT-Cre mice in the current study.

Funding

This work is supported by National Natural Science Foundation of China (82071495, 82271531 and 82211540400) and Traditional Chinese Medicine Technology Development Project of Jiangsu Province (ZD202302) to XWG, Natural Science Foundation of Nanjing University of Chinese Medicine (XZR2020019) to WZW and Jiangsu Basic Research Program Youth Fund Project (BK20210986) to QS.

Author contributions

Chen W, Guo H, Zhou N and Xu X performed the experiments and collected the data. Hu T and Mai Y performed the experiments and data analysis during the revision of the manuscript. Fan Y., Mai Y, and He T performed the data curation and analysis. Wen J, Qin S, Liu C and Wu W assist data analysis and some experiments. Fan Y, Ge F and Guan X prepared figures and wrote the draft. Kim HY edited the manuscript. Guan X, Liu C and Wu W raised the funding. Guan X conceptualized and supervised the project.

Data availability statement

The data that support the findings of this study are available from the corresponding author upon reasonable request.

Competing Interests

The authors have declared that no competing interest exists.

References

1. Su H, Zhang J, Ren W, Xie Y, Tao J, Zhang X, et al. Anxiety level and correlates in methamphetamine-dependent patients during acute withdrawal. Medicine (Baltimore). 2017; 96: e6434.
2. Xu X, Li N, Wen J, Yang P, Lu X, Wang Z, et al. Specific inhibition of interpeduncular nucleus GABAergic neurons alleviates anxiety-like behaviors in male mice after prolonged abstinence from methamphetamine. J Neurosci. 2023; 43: 803-11.
3. Campillo R. My experience and recovery from meth addiction. Missouri medicine. 2022; 119: 500.
4. Sun L, Liu R, Guo F, Wen MQ, Ma XL, Li KY, et al. Parabrachial nucleus circuit governs neuropathic pain-like behavior. Nat Commun. 2020; 11: 5974.
5. Geerling JC, Kim M, Mahoney CE, Abbott SB, Agostinelli LJ, Garfield AS, et al. Genetic identity of thermosensory relay neurons in the lateral parabrachial nucleus. Am J Physiol Regul Integr Comp Physiol. 2016; 310: R41-54.
6. Chiang MC, Nguyen EK, Canto-Bustos M, Papale AE, Oswald AM, Ross SE. Divergent neural pathways emanating from the lateral parabrachial nucleus mediate distinct components of the pain response. Neuron. 2020; 106: 927-39 e5.
7. Chiang MC, Bowen A, Schier LA, Tupone D, Uddin O, Heinricher MM. Parabrachial complex: a hub for pain and aversion. J Neurosci. 2019; 39: 8225-30.
8. Torres-Rodriguez JM, Wilson TD, Singh S, Torruella-Suarez ML, Chaudhry S, Adke AP, et al. The parabrachial to central amygdala pathway is critical to injury-induced pain sensitization in mice. Neuropsychopharmacology. 2024; 49:508-20.
9. Funahashi H, Pavlenko D, Sakai K, Verpile R, Sanders KM, Akiyama T. Dynorphinergic projections from the central amygdala to the parabrachial nucleus regulate itch. J Neurosci. 2023; 43: 5340-9.
10. Li JN, Wu XM, Zhao LJ, Sun HX, Hong J, Wu FL, et al. Central medial thalamic nucleus dynamically participates in acute itch sensation and chronic itch-induced anxiety-like behavior in male mice. Nat Commun. 2023; 14: 2539.
11. Hwang KD, Baek J, Ryu HH, Lee J, Shim HG, Kim SY, et al. Cerebellar nuclei neurons projecting to the lateral parabrachial nucleus modulate classical fear conditioning. Cell Rep. 2023; 42: 112291.
12. Chen CH, Newman LN, Stark AP, Bond KE, Zhang D, Nardone S, et al. A Purkinje cell to parabrachial nucleus pathway enables broad cerebellar influence over the forebrain. Nat Neurosci. 2023; 26: 1929-41.
13. Seiglie MP, Lepeak L, Miracle S, Cottone P, Sabino V. Stimulation of lateral parabrachial (LPB) to central amygdala (CeA) pituitary adenylate cyclase-activating polypeptide (PACAP) neurons induces anxiety-like behavior and mechanical allodynia. Pharmacol Biochem Behav. 2023; 230: 173605.
14. He T, Chen W, Fan Y, Xu X, Guo H, Li N, et al. A novel cholinergic projection from the lateral parabrachial nucleus and its role in methamphetamine-primed conditioned place preference. Brain Commun. 2022; 4: fcac219.
15. Jaramillo AA, Williford KM, Marshall C, Winder DG, Centanni SW. BNST transient activity associates with approach behavior in a stressful environment and is modulated by the parabrachial nucleus. Neurobiol Stress. 2020; 13: 100247.
16. Boucher MN, Aktar M, Braas KM, May V, Hammack SE. Activation of lateral parabrachial nucleus (LPBn) PACAP-expressing projection neurons to the bed nucleus of the stria terminalis (BNST) enhances anxiety-like behavior. J Mol Neurosci. 2022; 72: 451-8.
17. Williford KM, Taylor A, Melchior JR, Yoon HJ, Sale E, Negasi MD, et al. BNST PKCdelta neurons are activated by specific aversive conditions to promote anxiety-like behavior. Neuropsychopharmacology. 2023; 48: 1031-41.
18. Stamatakis AM, Sparta DR, Jennings JH, McElligott ZA, Decot H, Stuber GD. Amygdala and bed nucleus of the stria terminalis circuitry: implications for addiction-related behaviors. Neuropharmacology. 2014; 76 Pt B: 320-8.
19. Venniro M, Russell TI, Ramsey LA, Richie CT, Lesscher HMB, Giovanetti SM, et al. Abstinence-dependent dissociable central amygdala microcircuits control drug craving. Proc Natl Acad Sci U S A. 2020; 117: 8126-34.
20. Li X, Zeric T, Kambhampati S, Bossert JM, Shaham Y. The central amygdala nucleus is critical for incubation of methamphetamine craving. Neuropsychopharmacology. 2015; 40: 1297-306.
21. Lee KM, Coelho MA, Sern KR, Szumlinski KK. Homer2 within the central nucleus of the amygdala modulates withdrawal-induced anxiety in a mouse model of binge-drinking. Neuropharmacology. 2018; 128: 448-59.
22. Ferragud A, Velazquez-Sanchez C, Minnig MA, Sabino V, Cottone P. Pituitary adenylate cyclase-activating polypeptide (PACAP) modulates dependence-induced alcohol drinking and anxiety-like behavior in male rats. Neuropsychopharmacology. 2021; 46: 509-18.
23. Garcia-Carmona JA, Georgiou P, Zanos P, Bailey A, Laorden ML. Methamphetamine withdrawal induces activation of CRF neurons in the brain stress system in parallel with an increased activity of cardiac sympathetic pathways. Naunyn Schmiedebergs Arch Pharmacol. 2018; 391: 423-34.
24. Lucas-Meunier E, Monier C, Amar M, Baux G, Fregnac Y, Fossier P. Involvement of nicotinic and muscarinic receptors in the endogenous cholinergic modulation of the balance between excitation and inhibition in the young rat visual cortex. Cereb Cortex. 2009; 19: 2411-27.

25. Coronel-Oliveros C, Cofré R, Orio P. Cholinergic neuromodulation of inhibitory interneurons facilitates functional integration in whole-brain models. PLOS Computational Biology. 2021; 17: e1008737.
26. Picciotto MR, Higley MJ, Mineur YS. Acetylcholine as a neuromodulator: cholinergic signaling shapes nervous system function and behavior. Neuron. 2012; 76: 116-29.
27. Li X, Yu B, Sun Q, Zhang Y, Ren M, Zhang X, et al. Generation of a whole-brain atlas for the cholinergic system and mesoscopic projectome analysis of basal forebrain cholinergic neurons. Proceedings of the National Academy of Sciences. 2018; 115: 415-20.
28. Jaramillo AA, Brown JA, Winder DG. Danger and distress: parabrachial-extended amygdala circuits. Neuropharmacology. 2021; 198: 108757.
29. Liu S, Ye M, Pao GM, Song SM, Jhang J, Jiang H, et al. Divergent brainstem opioidergic pathways that coordinate breathing with pain and emotions. Neuron. 2022; 110: 857-73.e9.
30. Domi E, Xu L, Toivainen S, Wiskerke J, Coppola A, Holm L, et al. Activation of GABAB receptors in central amygdala attenuates activity of PKCδ + neurons and suppresses punishment-resistant alcohol self-administration in rats. Neuropsychopharmacology. 2023; 48: 1386-95.
31. Carter ME, Soden ME, Zweifel LS, Palmiter RD. Genetic identification of a neural circuit that suppresses appetite. Nature. 2013; 503: 111-4.
32. Miles OW, Thrailkill EA, Linden AK, May V, Bouton ME, Hammack SE. Pituitary adenylate cyclase-activating peptide in the bed nucleus of the stria terminalis mediates stress-Induced reinstatement of cocaine seeking in rats. Neuropsychopharmacology. 2018; 43: 978-86.
33. Perez RE, Basu A, Nabit BP, Harris NA, Folkes OM, Patel S, et al. alpha(2A)-adrenergic heteroreceptors are required for stress-induced reinstatement of cocaine conditioned place preference. Neuropsychopharmacology. 2020; 45: 1473-81.
34. McReynolds JR, Vranjkovic O, Thao M, Baker DA, Makky K, Lim Y, et al. Beta-2 adrenergic receptors mediate stress-evoked reinstatement of cocaine-induced conditioned place preference and increases in CRF mRNA in the bed nucleus of the stria terminalis in mice. Psychopharmacology (Berl). 2014; 231: 3953-63.
35. Shaham Y, Erb S, Stewart J. Stress-induced relapse to heroin and cocaine seeking in rats: a review. Brain Res Brain Res Rev. 2000; 33: 13-33.
36. Erb S, Stewart J. A role for the bed nucleus of the stria terminalis, but not the amygdala, in the effects of corticotropin-releasing factor on stress-induced reinstatement of cocaine seeking. J Neurosci. 1999; 19: RC35.
37. Wang J, Fang Q, Liu Z, Lu L. Region-specific effects of brain corticotropin-releasing factor receptor type 1 blockade on footshock-stress- or drug-priming-induced reinstatement of morphine conditioned place preference in rats. Psychopharmacology (Berl). 2006; 185: 19-28.
38. Leri F, Flores J, Rodaros D, Stewart J. Blockade of stress-induced but not cocaine-induced reinstatement by infusion of noradrenergic antagonists into the bed nucleus of the stria terminalis or the central nucleus of the amygdala. J Neurosci. 2002; 22: 5713-8.
39. Kalin NH, Shelton SE, Davidson RJ. The role of the central nucleus of the amygdala in mediating fear and anxiety in the primate. J Neurosci. 2004; 24: 5506-15.
40. Carvalho MC, Moreira CM, Zanoveli JM, Brandao ML. Central, but not basolateral, amygdala involvement in the anxiolytic-like effects of midazolam in rats in the elevated plus maze. J Psychopharmacol. 2012; 26: 543-54.
41. Neugebauer V, Li W, Bird GC, Han JS. The amygdala and persistent pain. Neuroscientist. 2004; 10: 221-34.
42. Raver C, Uddin O, Ji Y, Li Y, Cramer N, Jenne C, et al. An amygdalo-parabrachial pathway regulates pain perception and chronic pain. J Neurosci. 2020; 40: 3424-42.
43. Haubensak W, Kunwar PS, Cai H, Ciocchi S, Wall NR, Ponnusamy R, et al. Genetic dissection of an amygdala microcircuit that gates conditioned fear. Nature. 2010; 468: 270-6.
44. Hunt S, Sun Y, Kucukdereli H, Klein R, Sah P. Intrinsic circuits in the lateral central amygdala. eNeuro. 2017; 4.
45. Cai H, Haubensak W, Anthony TE, Anderson DJ. Central amygdala PKC-delta(+) neurons mediate the influence of multiple anorexigenic signals. Nat Neurosci. 2014; 17: 1240-8.
46. Tian G, Hui M, Macchia D, Derdeyn P, Rogers A, Hubbard E, et al. An extended amygdala-midbrain circuit controlling cocaine withdrawal-induced anxiety and reinstatement. Cell Rep. 2022; 39: 110775.
47. Xiao Q, Zhou X, Wei P, Xie L, Han Y, Wang J, et al. A new GABAergic somatostatin projection from the BNST onto accumbal parvalbumin neurons controls anxiety. Mol Psychiatry. 2021; 26: 4719-41.